Institute for Geophysics, Astrophysics, and Meteorology
University of Graz

RAP Research Group
Radiation and Air Pollution

IGAM/UG Technical Report for EU No. 1/2002

EDUCE
European Database for UV Climatology and Evaluation

[Contract No. EUK2-CT-1999-00028, WP 1.5]

Aerosol Climatology and Optical Properties of Key Aerosol Types Observed in Europe

by

S. Gonzi, D. Baumgartner, and E. Putz
(IGAM/University of Graz, Austria)

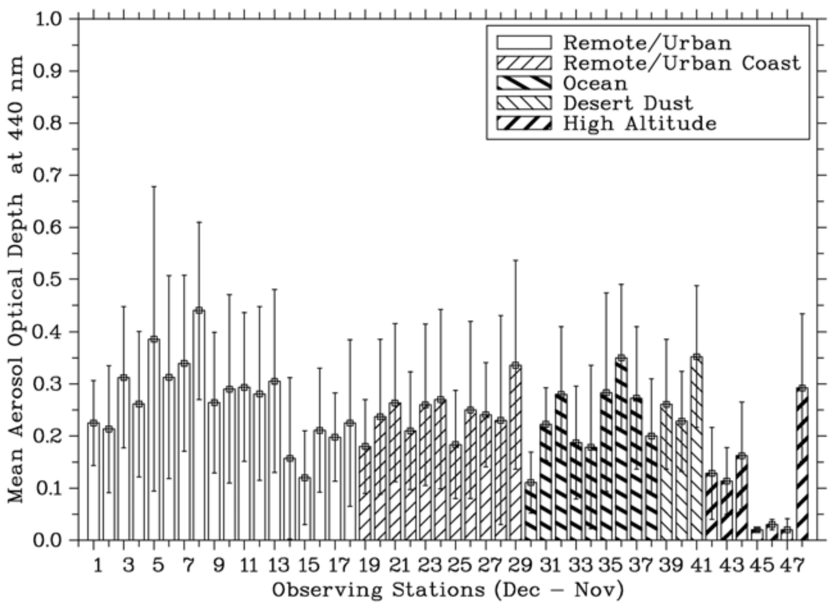

September 2002

Institute for Geophysics, Astrophysics, and Meteorology, University of Graz, Universitaetsplatz 5, A-8010 Graz, Austria
E-Mail: rap.igam@uni-graz.at, Web: http://www.uni-graz.at/igam/rap

Aerosol Climatology and Optical Properties of Key Aerosol Types Observed in Europe

Siegfried Gonzi, Dietmar Baumgartner, Erich Putz

October 7, 2002

Contents

1 Introduction

Aerosols have long played an important role in our understanding of climate forcing assessments (Penner *et al.*, 2001; Haywood and Boucher 2000). The greatest uncertainty in climate forcing is the contribution of aerosols (Lacis et al. 1992; Charlson *et al.*, 1999; Pilinis *et al.*, 1995; Nemesure *et al.*, 1995; Haywood and Ramaswamy 1998; Haywood and Shine 1995; Coakley *et al.* 1983). Monitoring and retrieving of aerosol optical properties is highly difficult. There are currently two methods to retrieve aerosol optical properties: satellite observations (Herman *et al.*, 1997a,b,c; King *et al.*, 1999; Torres *et al.*, 1998; Gonzalez *et al.*, 1997; Tanre *et al.*, 2001) and ground based measurements (cf. Hsu *et al.*, 1999; Husar *et al.*, 2000; Michalsky *et al.*, 2001; Remer *et al.*, 1998). Unlike greenhouse gases aerosols exhibit a strong temporal and spatial variation. Their influence on radiative forcing is dependent on solar zenith angle, surface albedo and wavelength (cf. Nemesure *et al.*, 1995). Most of the radiative forcing happens in the visible spectral range (cf. Coakley *et al.*, 1983). The influence of the infra-red regime, UV-band and beyond is in most cases negligible. But the UV region is beginning to become of interest for aerosol studies, especially the influence of areosols on radiation in the UV . Wenny *et al.*, 1998 report that the spectral UV-B transmission is correlated with optical depth. Mayer 1997 found that the transmission in the UV-A is negatively correlated with the aerosol optical depth. Some researchers assume even a higher influence of aerosols to UV radiation (Köpke 2002). In this paper we concentrate mainly upon the visible part of the solar spectrum, but discuss possibilities to extrapolate our findings into the UV band in order to include it for radiative forcing assessments. In the 90's the AERONET (Aerosol Robotic Network) network has been established in order to scrutinize the influence of aerosols upon climate. The network operates worldwide and uses an identical type of sunphotometer at every station (Holben *et al.*, 1998). The AERONET data are regularly used in order to contribute valuable results to the climate forcing discussion (Holben et. al 2001; Dubovik *et al.*, 2002; Eck *et al.*, 1999; Remer *et al.*, 1998). The AERONET network delivers the optical depth and in addition one can obtain the essential parameters for climate forcing studies: single scattering albedo; real part of refractive index; imaginary part of refractive index; particle size distribution. There are actually three classes (level 1.0, level 1.5, level 2.0) related to the accuracy of the AERONET data. Level 2.0 data are scarce, because they need a re-evaluation of the calibrated sunphotometer. Level 1.5 data are cloud screened (cf. Smirnov *et al.*, 2000) and quality assured to some degree. Level 1.0 data are real-time data and suited for applying own retrieval algorithms.

This report presents the statistical evaluation of the AERONET network operating over Europe. The report is exclusively based on level 1.5 data. It also discusses ideas to incorporate and extend the results into the UV regime.

2 Instrumentation

The recent development of scanning spectral radiometers, which automatically scan the direct and diffuse component of the solar spectrum, has enabled frequent measurements of atmospheric aerosol properties at remote sites. The sunphotometer which is applied in the AERONET network is a CIMEL radiometer CE-318. The method (cf. Holben *et al.*, 1998) to retrieve the optical depth follow the Beer-Lambert-Bouguer principle:

$$V_\lambda = V_0 d^2 e^{-\tau_\lambda m} t_y \qquad (1)$$

where V_λ... digital voltage; V_0... extraterrestrial voltage; m... optical airmass; τ... total optical depth; λ... wavelength; d... ratio of the average to the actual earth-sun distance; t_y... transmission of absorbing gases;

The CIMEL CE-318 is a solar powered weather hardy robotically pointed sun and sky spectral radiometer. It has 1.2° field of view and two detectors for measurements of direct sun, aureole and sky radiance.

Either direct sun or sky measurements are made in the range from 340 to 1020 nm. Every 15 minutes 3 measurements for each wavelength are performed. A triplet observation takes 1 minute. In addition sky measurements are made in order to assess the stability of the Langley plots.

More than four almucantar sequences are made daily at an optical airmass of 4, 3, 2 and 1.7, both morning and afternoon. An almucantar is a series of measurements taken at the elevation angle of the Sun for specified azimuth angles relative to the position of the Sun. Such an almucantar is made hourly between 9 am and 13 pm local solar time for the standard instrument, skipping only the noon almucantar for the polarization instrument. The standard principle plane sequence measures in much the same manner as the almucantar but in the principal plane of the sun where all angular distances from the sun are scattering angles regardless of solar zenith angle (cf. Holben 1998).

2.1 Instrument precision and accuracy

All instruments are routinely calibrated with Goddard's two meter integrating sphere at least twice per year. The absolute precision of the integrating sphere is about 5%. The sphere calibration procedure are then used to compute a gain and offset for each sky wavelength. The mean dark current is small (0 to 14 counts) under normal conditions. The extraterrestrial voltage V_0 is calculated from five or more Langley plots obtained at the Mauna Loa Observatory. It is not known exactly how the filters will alter with time, but a linear decay rate of the zero airmass voltage V_0 is assumed. To ensure stability, filters are changed every 2 years. Holben *et al.*, 1998 found that the absolute error after a newly calibrated instrument under cloud free conditions is lower than ± 0.01 for $\lambda > 440$ nm and lower than ± 0.02 for $\lambda < 440$ nm. The uncertainty in the water vapor channel (940 nm) is less than

12%. The sky radiance uncertainty is assumed to be less than $\pm 5\%$ for a newly calibrated system.

2.2 Screening Procedure

It is essential for climate studies to use the best calibration and instrument methods. This can only be assured with specific calibration methods. In addition to this technical issue it is important to use a cloud screening and quality control algorithm for the AERONET data base. Human observers can readily classify a wide range of cloudy skies, but an automatic network requires a different approach. The automatic sun/sky CIMEL radiometer CE-318 acquires data regardless of sky conditions. The radiometer makes only two basic measurements, either direct sun or diffuse radiances, bot within several programmed sequences.

Criterias used for the AERONET screening procedure (cf. Smirnov *et al.*, 2000):

1. Data quality checks: Aerosol optical depths lower than 0.01 are not accepted (the absolute value is at the same level as the calibration error). Also observations for air masses greater than 5 are not accepted (at low sun elevations the chance for cloudy conditions is high).

2. Triplet stability criteria: A triplet consists of three measurements (at any wavelength) over a total of a 1 minute period. If the total atmospheric column varies by more than 0.02 within one triplet then the measurement is considered not to be cloud free. If the triplet proof good the average of the three triplets is used as aerosol optical depth.

There are other more subtle points covering the screening procedure and the reader is referred to Smirnov *et al.*, 2000.

3 Aerosol Optical Properties

This section gives a short overview of relevant parameters in aerosol science.

One of the most important parameter in aerosol science is the optical depth. While the anthropogenic component amounts to only about 10% of the total, by mass, anthropogenic particles are estimated to produce as much as 50% of the global-mean aerosol optical depth (cf. Seinfeld and Pandis 1998). The extinction coefficient b_{ext} is a function of the particle size D_p, complex refractive index m and wavelength λ of the incident light (cf. Seinfeld and Pandis 1998 for an in depth textbook discussion):

$$b_{ext}(\lambda) = \int_0^{D_p^{max}} \frac{\pi D_p^2}{4} Q_{ext}(m, \alpha) n(D_p) dD_p \tag{2}$$

where D_p^{max} is an upper limit diameter for the particle population; $n(D_p)$ is the number size distribution function; $Q_{ext} = Q_{sca} + Q_{abs}$ is the dimensionless extinction efficiency and can be written in terms of the scattering Q_{sca} and absorption Q_{abs} efficiency; α is the well know dimensionless size parameter: $(\pi D_p)/\lambda$.

The optical depth is the integral of the extinction coefficient starting at height H_1 and ending at height H_2: $\tau = \int_{H_1}^{H_2} b_{ext}(\lambda)dh$. Note b_{ext} is the fractional loss of intensity per unit pathlength. The aerosol density distribution is not constant with height and shows a variation in the troposphere and to a lesser degree in the stratosphere. The model atmosphere is often divided into five height regions (cf. Krekov 1992):

1. The boundary layer (up to h_1 = 2 km), where the effect of the underlaying surface is considered to be the dominant factor
2. The turbulent mixing layer (h_2 = 2-4 km)
3. The background aerososl tropospheric layer with the top near the tropopause (from top of h_2 to h_3 = 4-12 km)
4. The stratospheric aerosol layer, including particulate material injected by volcanic eruptions extends between 12 and 30 km
5. The atmosphere above 30 km, is occupied with upper atmospheric aerosol including noctilucent clouds and meteoric debris

The AERONET network provides the column integrated aerosol optical depth and does not make any difference between different height levels. The column optical depth is appropiate for most of the radiative forcing assessments.

3.1 Particle Size Distribution

The size range of aerosol particles spans many orders of magnitude, so it is sensible to use a logarithmic scale when describing the distribution. The most often used parameter for describing the particle size distribution function is the aerosol volume distribution $n_V(D_p)$. According to Seinfeld and Pandis 1998:

$n_V(D_p)dD_p$ = the volume of particles per cm^3 of air having diameters in the range D_p to $D_p + dD_p$

It has been pointed out by several authors (cf. Hess *et al.*, 1998; Remer *et al.*, 1998) that the aerosol size distribution follows a bimodal log-normal distribution:

$$\frac{dV_i}{d\,lnr} = \frac{V_0}{\sigma(2\pi)^{1/2}} e^{-\frac{(ln(r/r_{m,i})^2)}{2\sigma^2}} \tag{3}$$

where $r_{m,i}$ is the related mode (median) radius for the accumulation or coarse mode (Remer et al. 1998); V_0 is the column volume of the particles per unit cross section of atmospheric column; σ is the standard deviation of the natural logarithm of the radius. The dimension of dV/d ln$r$ is [μm^3/μm^2]. The AERONET network retrieves the particle size distribution from the sunphotometer sky measurements in the almucantar and principal plane. An inversion algorithm is applied in order to calculate the optical properties (cf. Dubovik *et al.*, 2000).

3.2 Single Scattering Albedo

Incident light is scattered and absorbed by the particle. How much the light is absorbed is directly related to the single scattering albedo (cf. Seinfeld and Pandis 1998):

$$\omega = \frac{Q_{scat}}{Q_{ext}} = \frac{Q_{sca}}{Q_{sca} + Q_{abs}} \tag{4}$$

where Q_{sca} and Q_{abs} is the scattering and absorption efficiency per cross section of the particle, respectively. Q_{ext} can be written in terms of Q_{sca} and Q_{abs}. If ω is 1 the particle only scatters; if ω is 0 the particle is a perfect absorber. ω in combination with the upscatter fraction β determines whether heating or cooling of an aerosol layer will take place. Seinfeld and Pandis 1998 gives for the critical boundary between cooling and heating following relation:

$$\omega_{crit} = \frac{2R_s}{2R_s + \beta(1 - R_s)^2} \tag{5}$$

where R_s denotes the surface albedo; β is the upscatter fraction (cf. Boucher 1997; Wiscombe and Grams 1976). A typical global mean surface albedo R_s is about 0.15 and a representative value of the spectrally and solar zenith angle averaged β is about 0.29. According to these values the boundary between cooling and heating lies at 0.6. As will be shown with the AERONET data, low-value single scattering albedos are scarce.

4 Complex Refractive Index

The refractive index is especially important for judging the absorbtivity of the aerosol component. The absorption of a particle is related to the complex part of the refractive index. Pure water is almost completely transparent at visible wavelengths(cf. Krekov 1992), as opposed to soot, for which the imaginary part of the complex refractive index is large. There are two theories which are often used for describing the mixing state of aerosol compounds (cf. Seinfeld and Pandis 1998):

1. external mixture

2. internal mixture

In an external mixture every particle arises from only one source; in an internal mixture every particle is a uniform compound from each of the sources. The overall scattering coefficient for an internal- and external mixture is the same, however, the internal mixture shows a stronger absorption because every particle contributes to this process. But the extinction coefficient is normally higher for an external mixture. This observation is very important for assessing the radiative forcing because in most box models the single scattering albedo goes linear in the formula for the assessment (cf. Haywood and Shine 1995; Haywood and Ramaswamy 1998; Köpke 1992).

5 Results

5.1 Aerosol Optical Depth

The AERONET network has grown to a remarkable size, and has more than 45 stations in and around the border of Europe. The stations do not operate continuously, because of breaks for instrument calibration. Table 1 shows the location of the different AERONET stations. In addition to the geographical position and altitude there are class attributes in the first column, which are defined as follows:

R/U: Stations in remote and urban areas. It is essentially a mix of remote and urban areas. Because it is hard to draw a clear line between different classes a mix of different areas has been choosen instead.

R/UC: Stations in remote and coastlike urban areas. Marseille for example is in that class, though it is likely that others would group Marseille to R/U.

O: Stations in the ocean. This class is actually related to the maritime environment.

D: Stations in arid and desert like areas.

H: Stations above 1000 meters.

The definition of the classes is selective and is based on the geographical position. That will be not a great problem, because in the following chapters the results are presented for every location and not for every class alone. But it is feasible to include other criterias as well.

The CIMEL-CE 318 sunphotometer is capable of retrieving the aerosol optical depth at the wavelengths of 340/380/440/500/670/870/1020 nm. But not every station observes in all the wavelengths. The two most commonly observed wavelengths are at 440 and 870 nm. Figures 1 to 4 show the mean aerosol optical depth at 440 nm for every location and every quarter. The first quarter starts at the month of December; the last quarter ends in November. The shift compared to the normal year has been choosen in order to account for the meteorological season. To ensure a kind of stability the following statistical procedure has been applied in order to get the statistical parameters:

Table 1: AERONET Stations in Europe and beyond and their respective location. R/U. . . Remote/Urban ; R/UC. . . Remote/Urban Coast; O. . . Ocean; D. . . Desert; H. . . High Altitude. For the number of the respective observing station refer to this table in the following.

No.	Class	Station	Observer	Lat. [°]	Long. [°]	Alt. [m]
1	R/U	Aire Adour	Didier Tanre	N 43.7	E 0.3	80
2	R/U	Avignon	Michel Verbrugghe	N 43.9	E 4.9	32
30	O	Azores	Chuck McClain	N 38.5	W 28.6	50
19	R/UC	Biarritz	Philippe Goloub	N 43.5	W 1.6	0
20	R/UC	Bordeaux	Dominique Guyon	N 44.8	W 0.6	40
3	R/U	Bucharest	Didier Tanre	N 44.5	E 26.6	44
42	H	Clermont Ferrand	Didier Tanre	N 45.8	E 3.0	1464
31	O	Crete	Didier Tanre	N 35.3	E 25.7	140
4	R/U	Creteil	Bernadette Chatenet	N 48.8	E 2.4	57
43	H	Davos	Philippe Goloub	N 46.8	E 9.8	1596
32	O	Dead Sea	Rich Kleidman	N 31.1	E 35.5	-410
33	O	El Arenosillo	Victoria Cachorro Revilla	N 37.1	W 6.7	0
44	H	Gerlitzen	Dietmar Baumgartner	N 46.7	E 13.9	1900
34	O	Gotland	Bertil Hakansson	N 57.9	E 18.9	10
21	R/UC	Hamburg	Didier Tanre	N 53.6	E 10.0	105
35	O	Helgoland	Roland Doerffer	N 54.2	E 7.9	33
6	R/U	IFT Leipzig	Brent Holben	N 51.4	E 12.4	125
22	R/UC	IMC Oristano	Didier Tanre	N 39.9	E 8.5	10
39	D	IMS METU Erdemli	Chuck McClain	N 36.6	E 34.3	0
5	R/U	Ispra	Guiseppe Zibordi	N 45.8	E 8.6	235
45	H	Izana	Brent Holben	N 28.3	W 16.5	2367
36	O	Kolimbari	Jay Herman	N 35.5	E 23.8	0
37	R/UC	Lampedusa	Sergio Pugnaghi	N 35.5	E 12.6	45
7	R/U	Lille	Didier Tanre	N 50.6	E 3.1	60
23	R/UC	Marseille	Philippe Goloub	N 43.3	E 5.4	100
8	R/U	Modena	Sergio Pugnaghi	N 44.6	E 10.9	56
9	R/U	Moldova	Brent Holben	N 47.0	E 28.8	0
10	R/U	Moscow MSU MO	Brent Holben	N 55.7	E 37.5	50
11	R/U	Nes Ziona	Brent Holben	N 31.9	E 34.8	40
24	R/UC	Oostende	Jean P. DeBlauwe	N 51.2	E 2.9	30
12	R/U	Palaiseau	Bernadette Chatenet	N 48.7	E 2.2	156
46	H	Pic du Midi	Philippe Goloub	N 42.9	E 0.1	2898
25	R/UC	Rame Head	Samantha Lavender	N 50.4	W 4.1	0
26	R/UC	Realtor	Philippe Goloub	N 43.5	E 5.4	208
27	R/UC	Rome Tor Vergata	Gian Paolo Gobbi	N 41.8	E 12.6	130
13	R/U	Saclay	Patrick Chazette	N 48.7	E 2.2	160
40	D	Sede Boker	Brent Holben	N 30.5	E 34.5	480
14	R/U	SMHI	Bertil Hakansson	N 58.6	E 16.1	0
28	R/UC	Sopot	Brent Holben	N 54.5	E 18.6	0
41	D	Solar Village	Brent Holben	N 46.6	E 24.9	650
15	R/U	Tarbes	Philippe Goloub	N 43.3	E 0.1	350
47	H	Teide	Didier Tanre	N 28.3	W 16.6	3570
38	O	Tenerife	Brent Holben	N 28.0	W 16.6	10
48	H	Thala	Philippe Goloub	N 35.5	E 8.7	1091
16	R/U	Toulouse1	Didier Tanre	N 43.6	E 1.4	150
17	R/U	Toulouse2	Didier Tanre	N 43.6	E 1.5	150
29	R/UC	Venise	Guiseppe Zibordi	N 45.3	E 12.5	10
18	R/U	Vinon	Philippe Goloub	N 43.7	E 5.8	304

Table 2: The number of daily observations for every observing station and year. The quartely averages are based on the aerosol optical depth observations made in this months. Note the seasons start in December and end in November.

Year	Station	D	J	F	M	A	M	J	J	A	S	O	N
1995	Lille	-	-	-	11	-	-	-	12	-	-	5	-
	Sede Boker	-	-	-	-	23	11	-	-	-	6	23	15
1996	Aire Adour	-	-	-	-	-	11	18	17	17	19	16	6
	Crete	-	-	-	-	-	-	-	-	26	-	-	-
	Lille	-	-	-	-	10	-	-	-	-	-	-	-
	Sede Boker	-	-	15	22	25	26	22	26	25	13	-	5
	Venise	-	-	-	-	-	-	-	-	-	-	6	-
1997	Aire Adour	-	-	10	20	21	16	8	8	12	16	9	-
	Crete	-	-	-	-	-	17	21	28	-	-	-	-
	Ispra	-	-	-	-	-	-	-	20	18	17	22	13
	Izana	-	-	-	-	-	-	8	-	-	-	-	-
	Lille	-	5	-	-	13	10	8	9	19	5	-	-
	Rame Head	-	-	-	-	11	-	-	10	-	-	-	-
	Teide	-	-	-	-	-	-	14	22	-	-	-	-
	Teneriffe	-	-	-	-	-	-	-	19	-	-	-	-
	Venise	-	-	-	-	10	-	-	-	23	26	17	8
1998	Crete	-	-	9	-	-	-	-	-	-	-	-	-
	Ispra	5	11	19	20	12	23	20	21	27	19	7	-
	Rame Head	-	-	-	-	-	-	6	14	22	-	6	8
	Sede Boker	9	-	12	11	14	26	25	-	27	29	14	13
	Venise	-	-	11	11	5	23	18	23	-	13	8	13
1999	Clermont Ferrand	-	-	-	-	-	-	-	7	-	15	10	-
	Creteil	-	-	-	-	-	-	-	17	18	16	13	11
	Dead Sea	-	-	-	-	-	-	-	-	-	-	-	29
	Gotland	-	-	-	-	-	-	-	12	20	21	-	-
	Helgoland	-	-	-	5	12	12	-	-	-	-	-	-
	IMS METU Erdemli	-	-	-	-	-	-	-	-	-	-	-	10
	Ispra	-	-	-	-	-	-	19	23	20	19	12	18
	Kolimbari	-	-	-	-	-	9	-	-	-	-	-	-
	Lille	-	-	-	-	5	17	12	11	-	14	10	12
	Moldova	-	-	-	-	-	-	-	-	-	20	10	9
	Palaiseau	-	-	-	-	-	-	-	6	19	13	7	-
	Saclay	-	-	-	-	-	-	5	8	-	-	-	-
	Sede Boker	-	18	12	20	-	-	9	31	31	29	27	20
	Sopot	-	-	-	-	-	-	-	-	15	17	-	-
	Solar Village	-	-	6	29	29	31	29	31	31	28	27	29
	Toulouse1	-	-	-	-	-	-	-	8	18	22	15	11
	Toulouse2	-	-	-	-	-	-	-	-	-	5	12	11
	Venise	5	-	-	-	-	-	5	21	26	25	17	12

Table 3: Continuation of Table 2.

Year	Station	D	J	F	M	A	M	J	J	A	S	O	N
2000	Avignon	-	14	6	10	-	18	24	20	17	20	18	13
	Azores	-	-	-	-	-	-	12	17	27	23	21	19
	Bucharest	-	-	-	-	-	-	-	-	-	-	13	9
	Clermont Ferrand	-	-	-	-	-	12	-	-	-	-	-	-
	Creteil	-	-	-	-	-	-	-	9	21	21	8	-
	Dead Sea	25	-	-	-	-	-	-	-	-	-	-	-
	El Arenosillo	-	-	13	27	23	24	29	30	29	27	28	16
	Gotland	-	-	5	6	8	16	-	-	-	-	-	-
	Hamburg	-	-	-	-	-	-	6	8	12	11	11	-
	Helgoland	-	-	-	-	-	-	-	-	19	10	7	-
	IMC Oristano	-	-	-	-	-	-	26	31	31	27	24	16
	IMS METU Erdemli	22	15	15	26	21	27	30	30	31	29	26	26
	Ispra	13	23	21	21	11	16	24	20	25	22	8	-
	Lampedusa	-	-	-	-	-	-	-	31	29	16	-	-
	Lille	8	6	7	-	7	9	17	8	23	17	14	-
	Modena	-	-	-	-	-	5	-	-	-	-	-	-
	Moldova	8	7	11	9	19	31	25	-	-	-	-	-
	Nes Ziona	-	-	-	20	18	17	20	30	28	29	26	26
	Palaiseau	-	-	-	10	-	14	9	14	22	19	6	-
	Sede Boker	22	-	12	18	27	31	30	31	31	30	29	25
	Solar Village	-	-	-	-	21	30	30	31	31	30	31	15
	Toulouse1	6	10	16	16	-	-	-	-	-	6	9	13
	Toulouse2	7	5	11	16	16	-	-	-	-	-	-	-
	Venise	11	20	14	22	19	27	28	28	29	27	10	10
2001	Aire Adour	-	-	-	-	-	-	-	-	-	-	8	-
	Avignon	11	10	23	13	26	17	28	31	26	23	16	15
	Azores	7	-	11	15	16	12	14	15	17	11	12	7
	Biarritz	-	-	-	-	-	-	-	-	-	6	6	-
	Bordeaux	-	-	-	-	-	13	22	20	21	21	18	10
	Bucarest	6	6	17	16	19	20	23	26	31	-	-	-
	Creteil	-	-	5	-	-	-	-	-	-	-	-	-
	Davos	-	-	-	-	-	-	-	9	20	7	17	13
	El Arenosillo	12	17	19	17	19	20	25	18	27	22	21	23
	Gerlitzen	-	-	-	7	-	-	14	11	14	-	-	-
	Gotland	-	-	-	-	-	-	6	26	21	11	9	-
	Helgoland	-	-	-	-	-	-	-	11	11	-	-	-
	IFT Leipzig	-	-	-	-	-	5	12	21	18	7	14	6
	IMC Oristano	11	11	12	15	18	17	25	29	29	24	28	15
	IMS METU Erdemli	20	20	17	26	25	26	6	-	-	-	-	-
	Ispra	-	-	14	14	18	19	24	24	24	18	20	18
	Lille	9	14	9	5	10	24	22	14	20	6	11	12
	Marseille	-	-	-	-	-	-	21	17	-	-	-	-
	Moldova	-	-	-	-	-	22	17	24	29	16	20	12
	Moscow MSU	-	-	-	-	-	-	-	-	-	19	-	-
	Nes Ziona	16	23	16	28	28	26	30	31	6	-	-	-
	Oostende	-	-	-	-	-	-	10	18	24	9	11	6
	Pic du Midi	-	-	-	-	-	-	-	-	-	-	5	-
	Realtor	-	-	-	-	-	-	22	17	-	-	-	-
	Rome Tor Vergata	-	-	-	15	25	18	27	28	31	27	27	12
	Sede Boker	18	25	22	30	19	11	27	30	27	28	13	-
	SMHI	-	-	-	17	13	24	15	-	-	-	-	-
	Solar Village	8	24	19	23	29	31	30	31	25	27	28	26
	Tarbes	-	-	-	-	-	-	-	-	-	-	9	-
	Thala	-	-	-	6	20	22	29	31	28	22	26	-
	Toulouse1	7	-	16	10	14	-	18	21	23	18	25	10
	Venise	8	5	15	-	20	27	26	30	30	24	20	12
	Vinon	-	-	-	-	-	-	21	17	-	-	-	-

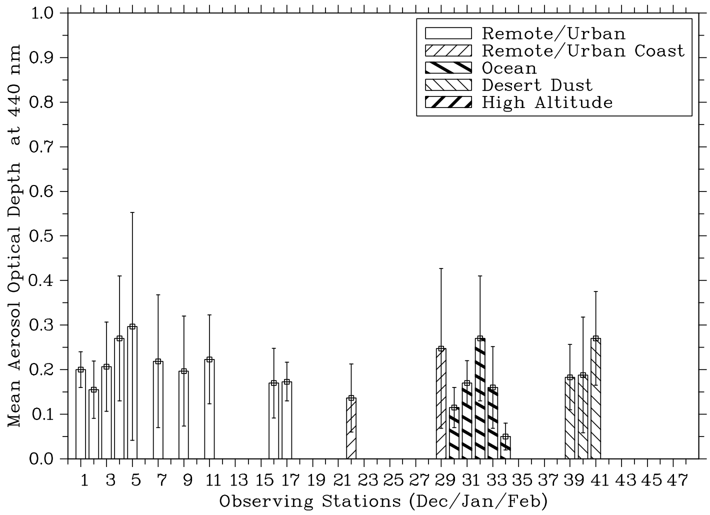

Figure 1: The quarterly average aerosol optical depth at 440 nm for every station – if present – for the 1. quarter. The error bars denote the standard deviation.

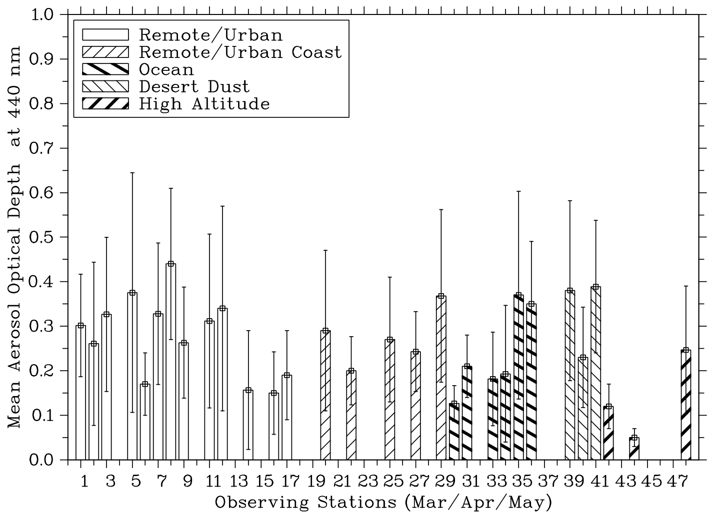

Figure 2: The quarterly average aerosol optical depth at 440 nm for every station – if present – for the 2. quarter. The error bars denote the standard deviation.

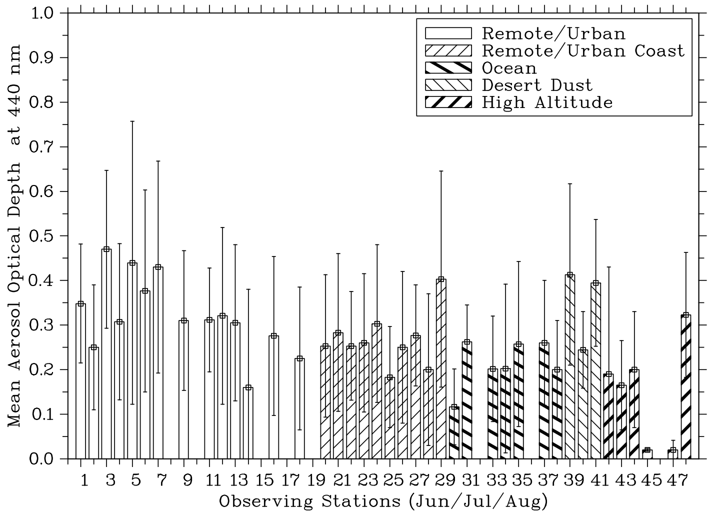

Figure 3: The quarterly average aerosol optical depth at 440 nm for every station – if present – for the 3. quarter. The error bars denote the standard deviation.

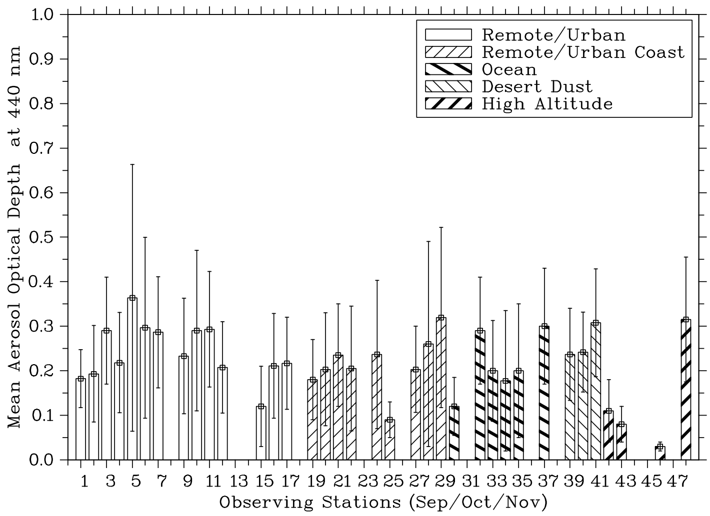

Figure 4: The quarterly average aerosol optical depth at 440 nm for every station – if present – for the 4. quarter. The error bars denote the standard deviation.

Table 4: Quarterly means of the aerosol optical depth at 440 nm for the complete class, respectively.

	1.Q.						2.Q.					
Class	N	Min	Med	Mean	Max	Std	N	Min	Med	Mean	Max	Std
R/U	10	0.10	0.18	0.21	0.43	0.11	13	0.11	0.25	0.28	0.65	0.16
R/UC	2	0.07	0.15	0.19	0.49	0.13	5	0.10	0.24	0.27	0.55	0.14
O	5	0.06	0.14	0.15	0.32	0.07	6	0.10	0.22	0.24	0.51	0.12
D	3	0.10	0.19	0.21	0.47	0.10	3	0.14	0.30	0.33	0.75	0.15
H. Alt.	-	-	-	-	-	-	3	0.07	0.11	0.14	0.30	0.07
	3.Q.						4.Q.					
Class	N	Min	Med	Mean	Max	Std	N	Min	Med	Mean	Max	Std
R/U	14	0.11	0.28	0.32	0.77	0.19	14	0.09	0.21	0.24	0.55	0.13
R/UC	10	0.08	0.22	0.27	0.63	0.16	9	0.08	0.17	0.21	0.55	0.13
O	7	0.08	0.18	0.21	0.53	0.13	6	0.08	0.18	0.21	0.51	0.12
D	3	0.17	0.32	0.35	0.72	0.14	3	0.13	0.24	0.26	0.55	0.10
H. Alt.	6	0.05	0.12	0.15	0.38	0.11	4	0.06	0.12	0.13	0.32	0.07

- A daily mean has been computed in the following, when there are at least 5 observation per day.
- If there are at least 5 daily means per month a monthly mean has been calculated.
- A mean for a quarter has been computed if there are one or more monthly means.
- In the following chapters the following denotions are used: N: Number of observations; Min: Minimum value; Med: Median value; Mean: Average value; Max: Maximum value; Std: Standard deviation;

The five observation threshold has been choosen in order to avoid possible outliers, which sometimes occur if there are only one or two measurements in a day. An average value for a typical year is based on the AERONET data set starting in 1995. But the main part of observations is made in the years 1999, 2000 and 2001. Table 2 shows the number of observations for every observing station and month. It is obvious that some stations do not cover every month and every year. One should bear this in mind, because the results presented here are based on the observations made in the months presented in Table 2.

Visual inspection of the Figures 1 to 4 show a clear trend insofar as that the aerosol optical depth is slightly higher in the second and third quarter. This is unsurprising, because the aerosol concentration is higher in the summer months than in the winter months. Michalsky *et al.*, 2001 reported from measurements made at nine stations in the eastern sector of the lower 48 United States for, at least, 4 years, with measurements continuing to this day at three of the sites. They found a remarkably increase in the aerosol optical depth in the summer months compared to winter months (for nearly all observing stations). Table 4 shows the average of the aerosol optical depth for every class and every quarter. The average is calculated from the means of the quarters for every station. In addition to the means the average minimum, maximum, median value and the standard deviation are included for every class.

It is obvious from Table 4 that the aerosol optical depth is higher in the summer months for all classes. For the remote/urban class the optical depth is about 50% higher in summer. The desert class and the remote/urban coast class exhibit also a slightly higher value for the aerosol optical depth in the summer months. Some high altitude aerosol optical depth values are very small, but even in high altitude remote areas (see the values for station 44 Gerlitzen) is the aerosol optical depth higher in the summer months than in the winter months.

There is no clear trend visible – except for the high altitude class – that the remote/urban class always exhibits the highest values. This is in great part due to the possible deliberate classification of the different locations. One should also bear in mind, that not every station delivers continuous observations. Nevertheless, Table 4 is a very important finding, especially for the modeler who wants to include the aerosol optical depth in a radiative forcing assessment. It can be said that in average the aerosol optical depth in Europe does not exceed a value of 0.35 and does not fall below 0.2 at 440 nm. One can also see from Table 4 that the remote/urban class has slightly higher mean optical depth values than the remote/urban coast class. This is mainly due to the fact that the aerosol optical depth is lower in coastal and in maritime environments. That finding fits together with the GADS data set (cf. Köpke *et al.*, 1997 for a description of the Global Aerosol Data Set). They show maps of optical depth values at 500 nm for an externally mixed aerosol, which exhibit lower optical depth values at coastlike areas in Europe.

As explained above, it is not possible to cover the whole of Europe with a measurement net. We tried to interpolate the quarterly and monthly mean aerosol optical depth values over Europe with the so called Kriging method. Kriging (cf. Kerry and Hawick 1998 for an application in high performance computing) is heavily used in earth science and some researchers have reported success in applying the Kriging interpolation to satellite ozone and aerosol data (cf. Guzzi 2001; Trachant 2000). In order to apply the Kriging scheme one needs an appropiate variogram. The variogram is a measure of quality for the continuity of a data set (cf. Isaaks 1989). A good variogram exhibits an exponential tendency. That means observing stations not far from each other have a strong correlation between data and observing stations far away from each other are not correlated. The variogram is a pre-condition for a successful (and meaningful) application of the Kriging algorithm. As it turned out with the AERONET data set, the variograms showed in most cases a weak linear relation. And some variograms exhibit moreover a random behavior (a horizontal straight line). Figure 5 shows a typical experimental variogram (cf. Isaaks 1989). It is obvious that the experimental variogram varies only slightly (see y-axis). That is due to the fact that the aerosol optical depth varies often only sligthly from one location to the next; especially there are AERONET stations which lie close together, which contribute to some kind of grouping of the locations. We tried different combinations of geographical grouping in order to get a more continuous placement of the observing stations, but the situation remains nearly the same, and the variogram is not useable.

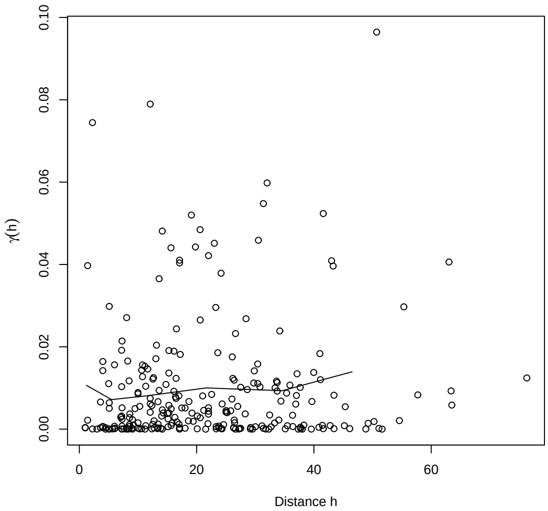

Figure 5: A typical experimental variogram for the AERONET data. The variogram shows the mean aerosol optical depth values for the month of June 2001. The variogram exhibits a weak linear relation; it would be highly questionable to use this variogram for the Kriging scheme. Other variograms for other months showed a similar behavior.

Another reason for the bad variogram could be that the aerosol optical depth rises or falls too abruptly from one location to the next. That means the variogram cannot see the variation between the locations and shows the situation for a randomly distributed data set. It is clear that in this situation an interpolation is meaningless.

There exist a couple of satellite projects which try to retrieve the aerosol optical depth from outside of the earth. We used the TOMS (cf. Herman *et al.*, 1997) satellite data in order to retrieve aerosol optical depth values over Europe for the last 20 years. The problem we encountered was that Europe is (after applying some statistical techniques for the daily and monthly means: there have to be more than 5 observations in a day; there have to be more than 5 days in a month for a monthly mean) nearly void of observations. The main part of observations is made over the equatorial regions.

Another prominent satellite project which delivers aerosol optical depth retrievals are the POLDER measurements (cf. Herman *et al.*, 1997). But the POLDER data cover only 9 months in the year of 1997. Hencefore we dropped the plan to investigate the POLDER data, because we searched for data, which cover at least one year and four seasons.

Table 5 shows the yearly average aerosol optical depth for each class. The trend is the same as for the quarterly means except for the high altitude class, which exhibits a low mean aerosol optical depth value.

Table 5: Yearly means of the aerosol optical depth at 440 nm for the complete class, respectively.

Class	N	Min	Med	Mean	Max	Std
R/U	18	0.10	0.23	0.27	0.61	0.15
R/UC	11	0.08	0.20	0.24	0.57	0.15
O	9	0.09	0.20	0.23	0.51	0.12
D	3	0.13	0.26	0.28	0.60	0.12
H. Alt.	7	0.05	0.09	0.11	0.26	0.06

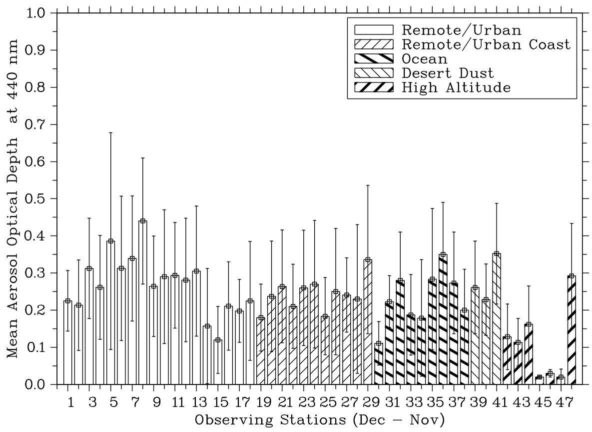

Figure 6: Yearly means of the average monthly means of the aerosol optical depth at 440 nm for every station. Error bars denote the standard deviation.

The mean aerosol optical depth values in Table 5 are based on the yearly means for each observing station and class. Figure 6 shows the mean aerosol optical depth averaged over the course of a year (from December to November). In addition to Figure 6, Table 6 exhibits the statistical values for every station. The yearly means are evaluated from the monthly means, which are in turn (as long as there are observation in past years) means from past years for every station.

6 The Ångström Coefficient α

The Ångström coefficient is of paramount interest for the climate forcing modeler, because most of the observations are made in the visible part of the solar spectrum, but one often wants to know the aerosol optical depth at shorter (or longer) wavelengths. It has proved to be useful to describe the wavelength dependence of the aerosol optical depth by the following relation:

Table 6: Yearly means of the average monthly means of the aerosol optical depth at 440 nm for every station.

Class	Station	Min	Med	Mean	Max	Std
Remote/Urban	Aire Adour	0.13	0.21	0.23	0.40	0.08
	Avignon	0.08	0.19	0.21	0.49	0.12
	Bucharest	0.14	0.29	0.31	0.64	0.14
	Creteil	0.10	0.23	0.26	0.53	0.14
	Ispra	0.07	0.31	0.39	1.11	0.29
	IFT Leipzig	0.13	0.23	0.31	0.69	0.19
	Lille	0.15	0.30	0.34	0.67	0.17
	Modena	0.16	0.49	0.44	0.60	0.17
	Moldova	0.09	0.23	0.26	0.57	0.14
	Moscow MSU	0.07	0.25	0.29	0.89	0.18
	Nes Ziona	0.11	0.27	0.29	0.72	0.14
	Palaiseau	0.10	0.26	0.28	0.66	0.17
	Saclay	0.12	0.27	0.31	0.57	0.17
	SMHI	0.05	0.10	0.16	0.63	0.16
	Tarbes	0.03	0.07	0.12	0.31	0.09
	Toulouse1	0.08	0.17	0.21	0.46	0.12
	Toulouse2	0.10	0.19	0.20	0.36	0.08
	Vinon	0.05	0.17	0.22	0.59	0.16
Remote/Urban Coast	Biarritz	0.12	0.14	0.18	0.35	0.09
	Bordeaux	0.09	0.19	0.24	0.63	0.15
	Hamburg	0.09	0.23	0.26	0.55	0.15
	IMC Oristano	0.08	0.18	0.21	0.53	0.11
	Marseille	0.08	0.20	0.26	0.54	0.16
	Oostende	0.10	0.21	0.27	0.65	0.17
	Rame Head	0.07	0.15	0.18	0.36	0.10
	Realtor	0.06	0.21	0.25	0.66	0.17
	Rome Tor Vergata	0.11	0.23	0.24	0.51	0.10
	Sopot	0.04	0.13	0.23	0.70	0.20
	Venise	0.09	0.30	0.34	0.79	0.20
Ocean	Azores	0.05	0.10	0.11	0.27	0.06
	Crete	0.10	0.23	0.22	0.37	0.07
	Dead Sea	0.11	0.23	0.28	0.66	0.13
	El Arenosillo	0.06	0.16	0.19	0.47	0.11
	Gotland	0.04	0.12	0.18	0.49	0.16
	Helgoland	0.12	0.24	0.28	0.73	0.19
	Kolimbari	0.16	0.36	0.35	0.57	0.14
	Lampedusa	0.10	0.24	0.27	0.63	0.14
	Tenerife	0.08	0.17	0.20	0.43	0.11
Desert	IMS Metu Erdemli	0.11	0.24	0.26	0.59	0.12
	Sede Boker	0.11	0.21	0.23	0.49	0.10
	Solar Village	0.17	0.33	0.35	0.72	0.14
High Altitude	Clermont Ferrand	0.05	0.09	0.13	0.31	0.09
	Davos	0.04	0.10	0.11	0.26	0.06
	Gerlitzen	0.06	0.14	0.16	0.41	0.10
	Izana	0.02	0.02	0.02	0.03	0.00
	Pic du Midi	0.02	0.03	0.03	0.05	0.01
	Teide	0.01	0.01	0.02	0.08	0.02
	Thala	0.12	0.26	0.29	0.66	0.14

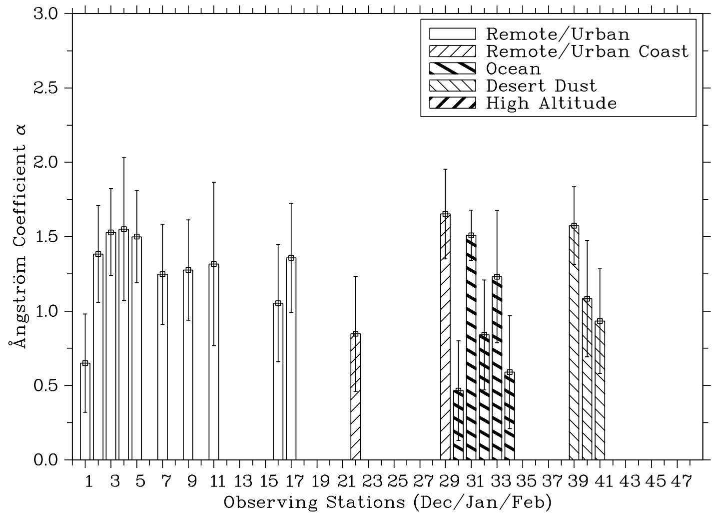

Figure 7: The quarterly average Ångström coefficient α – if present – for the 1. quarter. α is based on the aerosol optical depth observations at 440 and 870 nm. Error bars denote the standard deviation.

$$\tau(\lambda) \propto \lambda^{-\alpha} \tag{6}$$

If the optical depth is known at two wavelengths, the Ångström coefficient α can be obtained (cf. Seinfeld and Panis 1998):

$$\alpha = -\frac{log_{10}(\tau_1/\tau_2)}{log_{10}(\lambda_1/\lambda_2)} \tag{7}$$

We used the wavelengths at 440 and 870 nm in order to calculate α. Hess *et al.*, 1998 assume that α is not constant in the visible part of the solar spectrum and calculated α for the range of 350 - 500 nm and for the range of 500 - 800 nm, respectively. Nevertheless we assume that α is constant in the visible part of the solar spectrum.

Figures 7 to 10 show that α is slightly higher in the summer months. According to Dubovik *et al.*, 2000 a low α (down to 0) is a sign of large dust particles; a high α (up to 2) corresponds to small smoke particles. One can assume here that a higher aerosol optical depth is correlated with a higher Ångström coefficient due to combustion in motor vehicles, which is one of the predominant causes of air pollution in Europe.

Table 7 shows the quarterly means of the Ångström coefficient for every class (the calculation scheme is essentially the same as for the aerosol optical depth).

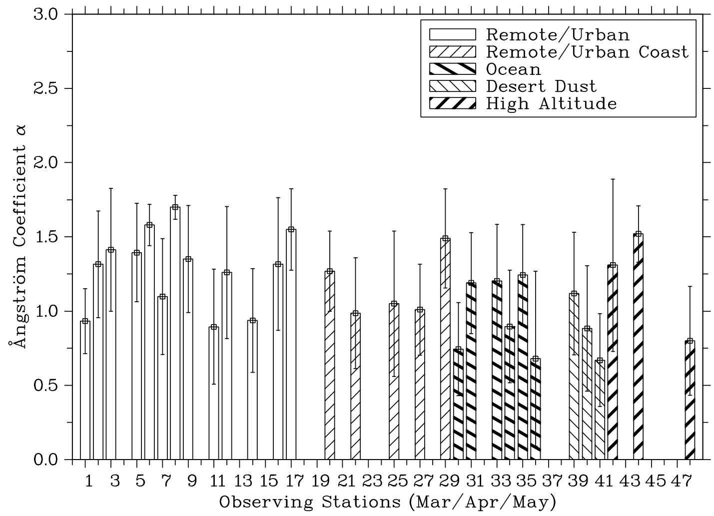

Figure 8: The quarterly average Ångström coefficient α – if present – for the 2. quarter. α is based on the aerosol optical depth observations at 440 and 870 nm. Error bars denote the standard deviation.

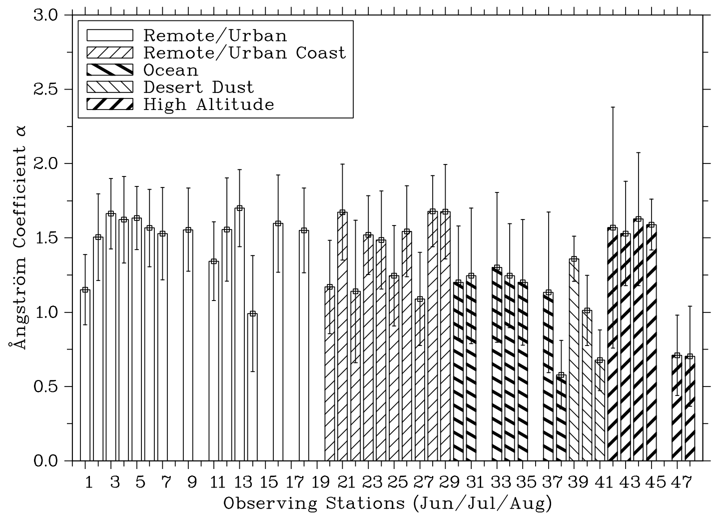

Figure 9: The quarterly average Ångström coefficient α – if present – for the 3. quarter. α is based on the aerosol optical depth observations at 440 and 870 nm. Error bars denote the standard deviation.

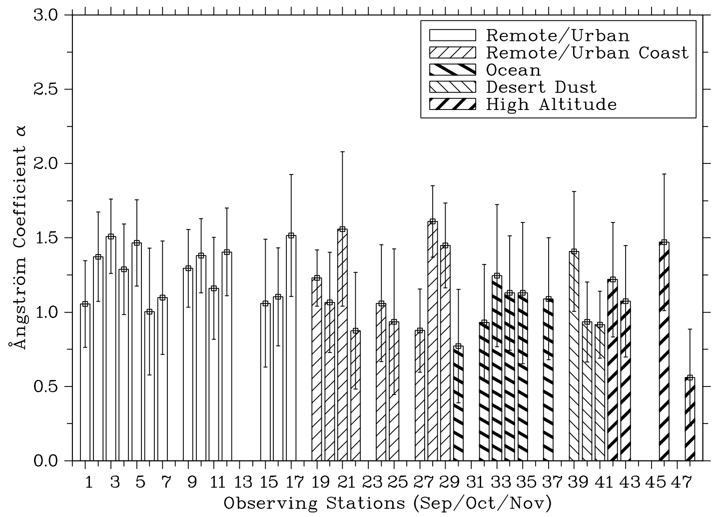

Figure 10: The quarterly average Ångström coefficient α – if present – for the 4. quarter. α is based on the aerosol optical depth observations at 440 and 870 nm. Error bars denote the standard deviation.

Table 7: Quarterly means of the Ångström coefficient for the complete class, respectively. α is based on the aerosol optical depth observations at 440 and 870 nm.

	1.Q.						2.Q.					
Class	N	Min	Med	Mean	Max	Std	N	Min	Med	Mean	Max	Std
R/U	10	0.60	1.35	1.29	1.74	0.37	13	0.66	1.33	1.29	1.75	0.32
R/UC	2	0.69	1.29	1.25	1.76	0.34	5	0.49	1.22	1.16	1.68	0.35
O	5	0.48	0.88	0.93	1.49	0.34	6	0.40	0.95	0.99	1.66	0.39
D	3	0.57	1.22	1.20	1.70	0.33	3	0.24	0.91	0.89	1.56	0.38
H. Alt.	-	-	-	-	-	-	3	0.59	1.31	1.21	1.66	0.38
	3.Q.						4.Q.					
Class	N	Min	Med	Mean	Max	Std	N	Min	Med	Mean	Max	Std
R/U	14	0.82	1.56	1.50	1.86	0.29	14	0.66	1.29	1.27	1.71	0.33
R/UC	10	0.73	1.47	1.42	1.88	0.32	9	0.55	1.22	1.18	1.68	0.35
O	7	0.43	1.14	1.13	1.80	0.41	6	0.28	1.13	1.05	1.62	0.42
D	3	0.60	1.03	1.02	1.35	0.20	3	0.47	1.14	1.09	1.51	0.30
H. Alt.	6	0.56	1.32	1.29	1.86	0.40	4	0.47	1.10	1.08	1.60	0.39

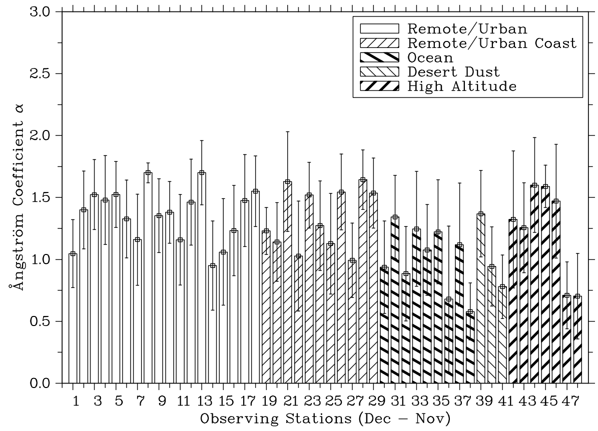

Figure 11: Yearly means of the average monthly means of the Ångström coefficient α for every station. α is based on the aerosol optical depth observations at 440 and 870 nm.

Table 8 gives the statistical parameters for every location. This table in combination with τ can be used to calculate the aerosol optical depth for the UV regime. The average α values are essentially above 1, except for the desert and ocean class. As has been said before a low α value corresponds to large particles, which correspond to the well known fact that arid and desert like areas have large dust like particles; sea salt particles are also thought to be of greater dimension than smoke particles.

Table 9 shows the average values for every different class. The trend is the same as for the quartely means, and it is obvious that the desert and ocean class has a much lower Ångström coefficient than the remote and urban classes. In order to get a better overview of the mean α values Figure 11 shows the mean α values for every class in a graphical depiction.

7 The Cumulative Frequency Distribution Function for the Aerosol Optical Depth and Ångström Coefficient α

Modelers often need a set of meaningful parameters in order to assess the climate forcing. The cumulative frequency distribution function (CFDF) can help insofar that one has a tool to to draw a border around reliable parameters. Figures 12 and 13 show the CFDF for the aerosol optical depth and Ångström coefficient α, respectively. For comparison the theoretical distribution function is alos depicted. The theoretical cumulative frequency distribution function is based on a Gaussian distribution:

Table 8: Yearly means of the average monthly means of the Ångström coefficient for every station. α is based on the aerosol optical depth observations at 440 and 870 nm.

	Station	Min	Med	Mean	Max	Std
Remote/Urban	Aire Adour	0.55	1.06	1.05	1.41	0.27
	Avignon	0.68	1.47	1.40	1.83	0.31
	Bucharest	0.86	1.59	1.52	1.85	0.28
	Creteil	0.80	1.52	1.48	1.94	0.36
	Ispra	0.92	1.56	1.52	1.88	0.27
	IFT Leipzig	0.73	1.37	1.33	1.70	0.31
	Lille	0.54	1.18	1.16	1.65	0.37
	Modena	1.59	1.70	1.70	1.79	0.08
	Moldova	0.71	1.42	1.35	1.73	0.30
	Moscow MSU	0.90	1.48	1.38	1.65	0.25
	Nes Ziona	0.43	1.19	1.16	1.72	0.37
	Palaiseau	0.86	1.51	1.46	1.91	0.35
	Saclay	1.30	1.74	1.70	1.99	0.26
	SMHI	0.25	1.00	0.95	1.56	0.36
	Tarbes	0.05	1.21	1.06	1.46	0.43
	Toulouse1	0.56	1.25	1.23	1.80	0.36
	Toulouse2	0.80	1.53	1.48	1.94	0.37
	Vinon	0.77	1.66	1.55	1.88	0.29
Remote/Urban Coast	Biarritz	0.97	1.27	1.23	1.47	0.19
	Bordeaux	0.49	1.19	1.14	1.60	0.32
	Hamburg	0.80	1.67	1.63	2.11	0.40
	IMC Oristano	0.28	1.01	1.03	1.82	0.44
	Marseille	0.85	1.56	1.52	1.89	0.27
	Oostende	0.66	1.30	1.27	1.76	0.36
	Rame Head	0.48	1.16	1.13	1.70	0.41
	Realtor	0.73	1.66	1.54	1.92	0.30
	Rome Tor Vergata	0.33	1.03	0.99	1.43	0.30
	Sopot	1.17	1.70	1.65	2.01	0.24
	Venise	0.92	1.60	1.53	1.91	0.28
Ocean	Azores	0.33	0.92	0.94	1.58	0.37
	Crete	0.76	1.34	1.34	1.81	0.34
	Dead Sea	0.15	0.80	0.89	1.46	0.38
	El Arenosillo	0.44	1.32	1.25	2.04	0.46
	Gotland	0.41	1.11	1.08	1.59	0.37
	Helgoland	0.47	1.34	1.22	1.72	0.42
	Kolimbari	0.29	0.38	0.68	1.84	0.59
	Lampedusa	0.32	1.12	1.12	1.95	0.50
	Tenerife	0.25	0.55	0.58	1.05	0.23
Desert	IMS Metu Erdemli	0.58	1.46	1.37	1.78	0.35
	Sede Boker	0.39	0.96	0.94	1.47	0.32
	Solar Village	0.33	0.77	0.78	1.28	0.26
High Altitude	Clermont Ferrand	0.27	1.49	1.32	1.98	0.55
	Davos	0.60	1.32	1.26	1.67	0.36
	Gerlitzen	0.83	1.70	1.60	2.02	0.38
	Izana	1.26	1.61	1.59	1.82	0.17
	Pic du Midi	0.94	1.51	1.47	2.03	0.46
	Teide	0.29	0.66	0.71	1.15	0.27
	Thala	0.17	0.67	0.70	1.30	0.35

Table 9: Yearly means of the average monthly means of the Ångström coefficient α for every station and every class, respectively. α is based on the aerosol optical depth measurements at 440 and 870 nm.

Class	N	Min	Med	Mean	Max	Std
R/C	18	0.74	1.41	1.36	1.76	0.31
R/UC	11	0.70	1.38	1.33	1.78	0.32
O	9	0.38	0.99	1.01	1.67	0.41
D	3	0.43	1.06	1.03	1.51	0.31
H. Alt.	7	0.62	1.28	1.24	1.71	0.36

$$f_n(x) = \frac{1}{\sqrt{2\pi}\sigma} e^{-\frac{x-\bar{x}}{2\sigma^2}} \tag{8}$$

The cumulative frequency distribution function for the observations follows the suggestion of Wilks 1995:

$$p(x_i) = \frac{i - \frac{1}{3}}{n + \frac{1}{3}} \tag{9}$$

where n is the number of observations and i is the index of observation.

The S-shaped distribution corresponds to values, which follow a gaussian distribution. That is especially important for the modelers, because the cumulative frequency distribution function is a representation of the propability density function.

8 Particle Size Distribution

In addition to the optical depth and Ångström coefficient the particle mode radius is of special interest for the climate forcing modeler. The mode radius is often used in combination with the Mie theory in order to calculate the upscatter fraction β and single scattering albedo ω. In turn this parameters are used to make an assessment of the radiative forcing (cf. Nemesure *et al.*, 1995). There exists actually two classes of mode radii (cf. Remer *et al.*, 1998):

accumulation mode: The mode radius – based on the volume distribution $dV/d\ \ln r$ – does not exceed 1 μm and lies normally between 0.1 - 1 μm

coarse mode: The mode radius – based on the volume distribution $dV/d\ \ln r$ – has values of many micrometers ($>$ 1 μm)

The AERONET network retrieves the particle size distribution with an inversion algorithm based on the model of polydispersed homogeneous spheres (cf. Dubovik *et al.*, 2000). Dubovik *et al.*, 2000 reported from retrieval errors up to

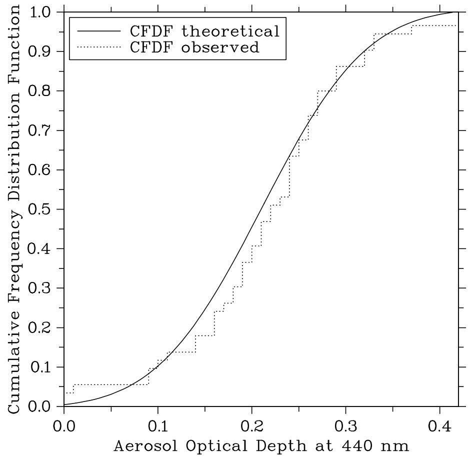

Figure 12: The cumulative frequency distribution function for the mean yearly aerosol optical depth values. The CFDF has been evaluated from the average yearly aerosol optical depth values for every station. The theoretical distribution has the parameters: mean = 0.23; σ = 0.09.

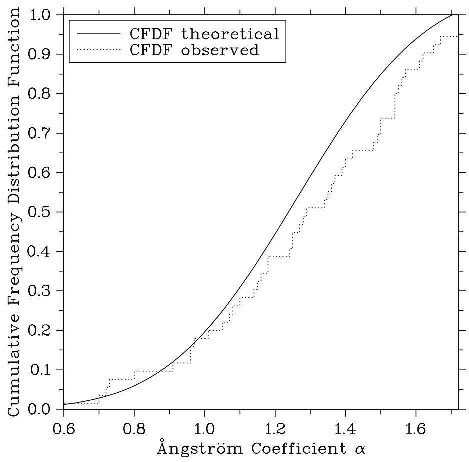

Figure 13: The cumulative frequency distribution function for the mean yearly Ångström coefficient α. The CFDF has been evaluated from the average yearly Ångström coefficient α for every station. The theoretical distribution has the parameters: mean = 1.25; σ = 0.29.

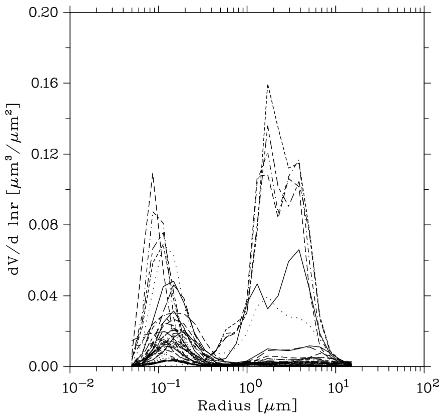

Figure 14: dV/d ln$r$ for the Gerlitzen station of the year 2001. Two mode classes: fine and coarse mode are predominant.

100% at the boundaries (0.05 - 0.1 and 7 - 15 μm). As it will be demonstrated the fine mode particle size radius is above 0.1 μm and the coarse mode particle radius is below 7 μm. Errors at the boundary are, therefore, of minor concern. But there exist situations when the behavior is unsatisfactory and may lead to difficulties in interpretation (see the Bucharest example below, which will follow).

Figure 14 shows the dV/d ln$r$ retrievals of the Gerlitzen station. It is obvious that the fine mode and coarse mode radius varies remarkably; in order to get a mean median value it is essential to use the following statistical methods (cf. Dubovik *et al.*, 2000):

The volume median radius computed for both fine and coarse modes:

$$ln\, r_V = \frac{\int_{r_{min}}^{r_{max}} ln\, r \frac{dV(r)}{d\, lnr} d\, lnr}{\int_{r_{min}}^{r_{max}} \frac{dV(r)}{d\, lnr} d\, lnr} \tag{10}$$

Standard deviation from the volume median radius:

$$\sigma_V = \sqrt{\frac{\int_{r_{min}}^{r_{max}} (lnr - lnr_V)^2 \frac{dV(r)}{d\, lnr} d\, lnr}{\int_{r_{min}}^{r_{max}} \frac{dV(r)}{d\, lnr} d\, lnr}} \tag{11}$$

Volume concentration [μm^3/μm^2]:

$$C_V = \int_{r_{min}}^{r_{max}} \frac{dV(r)}{d\, lnr} d\, lnr \tag{12}$$

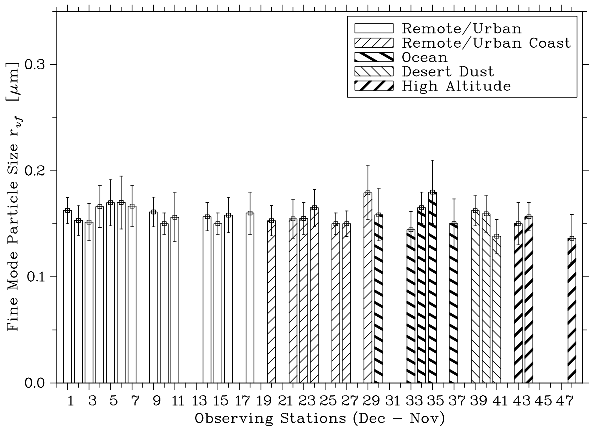

Figure 15: The fine mode radius for every station. Error bars denote the standard deviation.

In order to use the radii for climate modeling, we present in Table 10 and 11 the yearly average mode radius for every station. Tables 12 to 15 show the standard deviation and the volume concentration for the fine and coarse mode, respectively.

As one can see the mode radii for the different obserbing stations are nearly as constant over Europe (consult also Figures 15 and 16 for a graphical representation). The modeler is not only interested in the mode radius alone, also of special interest is the average standard deviation (which describes the width of the distribution). In climate modeling a log-normal distribution is often applied with a mean mode radius and a respective standard deviation. In the literature the standard deviation is often estimated based on experience and reasoning.

This does not mean, however, that there are identical particle compositions at every observing station. Most of the particles over Europe are the result of combustion processes and biomass burning. This is also evident in the single scattering albedo which is then lower than 1 and some kind of absorption takes place, which is unsurprising because soot is thought to become produced in combination with sulfur. As it has been pointed out a high Ångström coefficient is correlated with a high concentration of coarse particles and a small Ångström coefficient is connected with small smoke particles. One can refer to Figures 17 and 18 in order to evaluate the aforementioned relation.

It was demonstrated that the mode radii do not vary that much from station to station. We present therefore the yearly means of the statistical parameters for every class only. Tables 16 to 19 include the mode radius and the respective standard deviation and volume concentrations . Figure 19 exhibits the cumulative frequency distribution function for the important parameters: mode radius, standard deviation from the median radius and volume concentration for the fine and coarse mode, re-

Table 10: Yearly means of the average monthly means of the median mode radius for the volume particle size distribution for the finde mode and for every station.

	Station	Min	Med	Mean	Max	Std
Remote/Urban	Aire Adour	0.15	0.16	0.16	0.18	0.01
	Avignon	0.14	0.15	0.15	0.18	0.01
	Bucharest	0.13	0.16	0.15	0.18	0.02
	Creteil	0.14	0.16	0.17	0.19	0.02
	Ispra	0.14	0.17	0.17	0.21	0.02
	IFT Leipzig	0.13	0.17	0.17	0.20	0.03
	Lille	0.14	0.17	0.17	0.20	0.02
	Modena	-	-	-	-	-
	Moldova	0.14	0.16	0.16	0.19	0.01
	Moscow MSU	0.13	0.15	0.15	0.17	0.01
	Nes Ziona	0.12	0.16	0.16	0.20	0.02
	Palaiseau	-	-	-	-	-
	Saclay	-	-	-	-	-
	SMHI	0.14	0.16	0.16	0.18	0.01
	Tarbes	0.14	0.15	0.15	0.16	0.01
	Toulouse1	0.14	0.16	0.16	0.18	0.02
	Toulouse2	-	-	-	-	-
	Vinon	0.14	0.16	0.16	0.20	0.02
Remote/Urban Coast	Biarritz	-	-	-	-	-
	Bordeaux	0.13	0.15	0.15	0.18	0.01
	Hamburg	-	-	-	-	-
	IMC Oristano	0.12	0.15	0.15	0.18	0.02
	Marseille	0.13	0.16	0.16	0.19	0.01
	Oostende	0.15	0.17	0.17	0.20	0.02
	Rame Head	-	-	-	-	-
	Realtor	0.13	0.15	0.15	0.17	0.01
	Rome Tor Vergata	0.13	0.15	0.15	0.18	0.01
	Sopot	-	-	-	-	-
	Venise	0.14	0.18	0.18	0.22	0.03
Ocean	Azores	0.13	0.15	0.16	0.20	0.02
	Crete	-	-	-	-	-
	Dead Sea	-	-	-	-	-
	El Arenosillo	0.12	0.14	0.14	0.18	0.02
	Gotland	0.15	0.17	0.17	0.19	0.01
	Helgoland	0.14	0.18	0.18	0.22	0.03
	Kolimbari	-	-	-	-	-
	Lampedusa	0.12	0.15	0.15	0.20	0.02
	Tenerife	-	-	-	-	-
Desert	IMS Metur Erdemli	0.14	0.16	0.16	0.19	0.01
	Sede Boker	0.13	0.16	0.16	0.19	0.02
	Solar Village	0.11	0.14	0.14	0.17	0.02
High Altitude	Clermont Ferrand	-	-	-	-	-
	Davos	0.13	0.15	0.15	0.19	0.02
	Gerlitzen	0.14	0.15	0.16	0.18	0.01
	Izana	-	-	-	-	-
	Pic du Midi	-	-	-	-	-
	Teide	-	-	-	-	-
	Thala	0.10	0.13	0.14	0.17	0.02

Table 11: Yearly means of the average monthly means of the median mode radius for the volume particle size distribution for the coarse mode and for every station.

	Station	Min	Med	Mean	Max	Std
Remote/Urban	Aire Adour	2.1	2.6	2.7	3.3	0.4
	Aviharest	2.1	2.9	3.0	4.2	0.6
	Bucarest	2.5	3.1	3.1	3.6	0.4
	Creteil	2.4	2.9	3.0	4.0	0.6
	Ispra	2.4	3.2	3.2	4.1	0.5
	IFT Leipzig	2.0	3.0	3.0	4.2	0.7
	Lille	2.2	2.9	2.9	3.4	0.4
	Modena	-	-	-	-	-
	Moldova	2.2	3.2	3.2	4.1	0.6
	Moscow MSU	2.3	3.1	2.9	3.4	0.4
	Nes Ziona	1.8	2.5	2.5	3.3	0.4
	Palaiseau	-	-	-	-	-
	Saclay	-	-	-	-	-
	SMHI	1.7	2.5	2.5	3.5	0.5
	Tarbes	2.3	2.6	2.7	3.3	0.4
	Toulouse1	2.3	2.9	2.9	3.8	0.5
	Toulouse2	-	-	-	-	-
	Vinon	2.3	3.2	3.1	3.8	0.5
Remote/Urban Coast	Biarritz	-	-	-	-	-
	Bordeaux	2.1	2.9	2.9	3.6	0.5
	Hamburg	-	-	-	-	-
	IMC Oristano	2.1	2.7	2.8	3.7	0.5
	Marseille	2.4	3.1	3.1	3.6	0.4
	Oostende	2.2	2.9	2.9	3.6	0.5
	Rame Head	-	-	-	-	-
	Realtor	1.6	2.5	2.4	2.7	0.3
	Rome Tor Vergata	2.0	2.8	2.9	3.8	0.5
	Sopot	-	-	-	-	-
	Venise	2.2	3.1	3.1	4.2	0.6
Ocean	Azores	1.9	2.4	2.5	3.6	0.6
	Crete	-	-	-	-	-
	Dead Sea	-	-	-	-	-
	El Arenosillo	1.9	2.5	2.5	3.4	0.4
	Gotland	2.3	3.4	3.5	5.3	0.8
	Helgoland	2.2	3.2	3.1	3.7	0.5
	Kolimbari	-	-	-	-	-
	Lampedusa	1.9	2.5	2.6	3.3	0.4
	Tenerife	-	-	-	-	-
Desert	IMS Metu Erdemli	2.1	3.1	3.1	4.0	0.6
	Sede Boker	2.0	2.5	2.6	3.7	0.5
	Solar Village	2.0	2.3	2.3	2.8	0.2
High Altitude	Clermont Ferrand	-	-	-	-	-
	Davos	1.9	2.7	2.8	5.4	1.1
	Gerlitzen	2.0	2.3	2.3	2.7	0.3
	Izana	-	-	-	-	-
	Pic du Midi	-	-	-	-	-
	Teide	-	-	-	-	-
	Thala	2.0	2.4	2.6	3.7	0.5

Table 12: Yearly means of the average monthly means of the standard deviation of the median radius of the volume particle size distribution of the fine mode and for every station.

	Station	Min	Med	Mean	Max	Std
Remote/Urban	Aire Adour	0.30	0.33	0.33	0.38	0.03
	Avignon	0.32	0.35	0.36	0.41	0.03
	Bucharest	0.32	0.35	0.36	0.43	0.04
	Creteil	0.35	0.38	0.38	0.43	0.03
	Ispra	0.31	0.36	0.36	0.42	0.03
	IFT Leipzig	0.32	0.38	0.39	0.45	0.04
	Lille	0.33	0.37	0.38	0.44	0.04
	Modena	-	-	-	-	-
	Moldova	0.30	0.35	0.35	0.41	0.03
	Moscow MSU	0.31	0.34	0.34	0.39	0.03
	Nes Ziona	0.28	0.35	0.35	0.42	0.04
	Palaiseau	-	-	-	-	-
	Saclay	-	-	-	-	-
	SMHI	0.31	0.34	0.34	0.39	0.02
	Tarbes	0.32	0.35	0.36	0.42	0.04
	Toulouse1	0.32	0.37	0.37	0.42	0.04
	Toulouse2	-	-	-	-	-
	Vinon	0.30	0.34	0.34	0.39	0.03
Remote/Urban Coast	Biarritz	-	-	-	-	-
	Bordeaux	0.32	0.36	0.36	0.43	0.03
	Hamburg	-	-	-	-	-
	IMC Oristano	0.33	0.38	0.39	0.48	0.05
	Marseille	0.34	0.39	0.40	0.46	0.04
	Oostende	0.34	0.38	0.39	0.46	0.04
	Rame Head	-	-	-	-	-
	Realtor	0.30	0.33	0.34	0.42	0.03
	Rome Tor Vergata	0.30	0.34	0.34	0.43	0.04
	Sopot	-	-	-	-	-
	Venise	0.34	0.38	0.38	0.44	0.03
Ocean	Azores	0.31	0.38	0.38	0.46	0.05
	Crete	-	-	-	-	-
	Dead Sea	-	-	-	-	-
	El Arenosillo	0.30	0.36	0.36	0.45	0.04
	Gotland	0.33	0.38	0.38	0.44	0.04
	Helgoland	0.31	0.36	0.37	0.42	0.04
	Kolimbari	-	-	-	-	-
	Lampedusa	0.33	0.40	0.40	0.48	0.04
	Tenerife	-	-	-	-	-
Desert	IMS Metu Erdemli	0.30	0.33	0.33	0.39	0.03
	Sede Boker	0.31	0.37	0.37	0.45	0.04
	Solar Village	0.29	0.36	0.37	0.46	0.04
High Altitude	Clermont Ferrand	-	-	-	-	-
	Davos	0.34	0.38	0.37	0.41	0.02
	Gerlitzen	0.32	0.36	0.37	0.41	0.03
	Izana	-	-	-	-	-
	Pic du Midi	-	-	-	-	-
	Teide	-	-	-	-	-
	Thala	0.32	0.42	0.43	0.54	0.07

Table 13: Yearly means of the average monthly means of the standard deviation of the median radius of the volume particle size distribution of the coarse mode and for every station.

	Station	Min	Med	Mean	Max	Std
Remote/Urban	Aire Adour	0.59	0.68	0.69	0.81	0.08
	Avignon	0.64	0.75	0.75	0.85	0.06
	Bucharest	0.64	0.72	0.72	0.80	0.05
	Creteil	0.65	0.70	0.71	0.79	0.05
	Ispra	0.64	0.73	0.73	0.84	0.06
	IFT Leipzig	0.54	0.73	0.72	0.90	0.12
	Lille	0.64	0.74	0.75	0.89	0.08
	Modena	-	-	-	-	-
	Moldova	0.62	0.72	0.71	0.81	0.06
	Moscow MSU	0.60	0.68	0.67	0.72	0.04
	Nes Ziona	0.52	0.62	0.62	0.72	0.05
	Palaiseau	-	-	-	-	-
	Saclay	-	-	-	-	-
	SMHI	0.65	0.76	0.75	0.87	0.06
	Tarbes	0.66	0.77	0.76	0.81	0.06
	Toulouse1	0.60	0.69	0.69	0.80	0.07
	Toulouse2	-	-	-	-	-
	Vinon	0.63	0.69	0.71	0.80	0.06
Remote/Urban Coast	Biarritz	-	-	-	-	-
	Bordeaux	0.64	0.74	0.73	0.82	0.06
	Hamburg	-	-	-	-	-
	IMC Oristano	0.58	0.67	0.67	0.74	0.05
	Marseille	0.61	0.70	0.70	0.79	0.04
	Oostende	0.62	0.70	0.70	0.80	0.06
	Rame Head	-	-	-	-	-
	Realtor	0.50	0.63	0.63	0.78	0.07
	Rome Tor Vergata	0.61	0.70	0.70	0.82	0.06
	Sopot	-	-	-	-	-
	Venise	0.65	0.76	0.76	0.89	0.07
Ocean	Azores	0.57	0.67	0.66	0.77	0.07
	Crete	-	-	-	-	-
	Dead Sea	-	-	-	-	-
	El Arenosillo	0.57	0.66	0.66	0.76	0.06
	Gotland	0.64	0.73	0.73	0.84	0.06
	Helgoland	0.39	0.56	0.60	0.86	0.17
	Kolimbari	-	-	-	-	-
	Lampedusa	0.57	0.64	0.64	0.73	0.05
	Tenerife	-	-	-	-	-
Desert	IMS Metu Erdemli	0.59	0.69	0.69	0.78	0.05
	Sede Boker	0.57	0.65	0.66	0.76	0.05
	Solar Village	0.53	0.59	0.60	0.66	0.04
High Altitude	Clermont Ferrand	-	-	-	-	-
	Davos	0.59	0.72	0.75	0.93	0.12
	Gerlitzen	0.64	0.78	0.77	0.89	0.09
	Izana	-	-	-	-	-
	Pic du Midi	-	-	-	-	-
	Teide	-	-	-	-	-
	Thala	0.57	0.68	0.68	0.82	0.07

Table 14: Yearly means of the average monthly means of the volume concentration of the volume particle size distribution of the fine mode and for every station.

	Station	Min	Med	Mean	Max	Std
Remote/Urban	Aire Adour	0.03	0.05	0.06	0.11	0.03
	Avignon	0.01	0.03	0.03	0.06	0.02
	Bucharest	0.01	0.04	0.04	0.08	0.02
	Creteil	0.01	0.03	0.03	0.07	0.02
	Ispra	0.01	0.04	0.05	0.11	0.03
	IFT Leipzig	0.02	0.07	0.07	0.12	0.04
	Lille	0.03	0.06	0.06	0.12	0.03
	Modena	-	-	-	-	-
	Moldova	0.01	0.03	0.04	0.08	0.02
	Moscow MSU	0.01	0.04	0.04	0.07	0.02
	Nes Ziona	0.01	0.03	0.03	0.07	0.02
	Palaiseau	-	-	-	-	-
	Saclay	-	-	-	-	-
	SMHI	0.01	0.01	0.02	0.03	0.01
	Tarbes	0.01	0.01	0.01	0.03	0.01
	Toulouse1	0.01	0.03	0.03	0.07	0.02
	Toulouse2	-	-	-	-	-
	Vinon	0.01	0.02	0.03	0.06	0.01
Remote/Urban Coast	Biarritz	-	-	-	-	-
	Bordeaux	0.01	0.02	0.03	0.07	0.02
	Hamburg	-	-	-	-	-
	IMC Oristano	0.01	0.02	0.02	0.05	0.01
	Marseille	0.01	0.03	0.04	0.11	0.03
	Oostende	0.01	0.03	0.04	0.08	0.02
	Rame Head	-	-	-	-	-
	Realtor	0.01	0.02	0.03	0.08	0.02
	Rome Tor Vergata	0.01	0.03	0.03	0.06	0.01
	Sopot	-	-	-	-	-
	Venise	0.01	0.04	0.04	0.10	0.03
Ocean	Azores	0.01	0.01	0.01	0.03	0.01
	Crete	-	-	-	-	-
	Dead Sea	-	-	-	-	-
	El Arenosillo	0.01	0.02	0.02	0.05	0.01
	Gotland	0.00	0.01	0.02	0.07	0.02
	Helgoland	0.01	0.04	0.04	0.09	0.03
	Kolimbari	-	-	-	-	-
	Lampedusa	0.01	0.03	0.03	0.06	0.02
	Tenerife	-	-	-	-	-
Desert	IMS Metu Erdemli	0.01	0.04	0.04	0.07	0.02
	Sede Boker	0.01	0.02	0.02	0.05	0.01
	Solar Village	0.01	0.02	0.03	0.06	0.01
High Altitude	Clermont Ferrand	-	-	-	-	-
	Davos	0.01	0.01	0.01	0.03	0.01
	Gerlitzen	0.01	0.01	0.02	0.04	0.01
	Izana	-	-	-	-	-
	Pic du Midi	-	-	-	-	-
	Teide	-	-	-	-	-
	Thala	0.01	0.02	0.02	0.04	0.01

Table 15: Yearly means of the average monthly means of the volume concentration of the volume particle size distribution of the coarse mode and for every station.

	Station	Min	Med	Mean	Max	Std
Remote/Urban	Aire Adour	0.01	0.02	0.03	0.06	0.02
	Avignon	0.01	0.02	0.03	0.07	0.02
	Bucharest	0.01	0.02	0.03	0.10	0.03
	Creteil	0.01	0.02	0.03	0.06	0.02
	Ispra	0.01	0.02	0.03	0.10	0.03
	IFT Leipzig	0.03	0.04	0.07	0.23	0.07
	Lille	0.02	0.03	0.03	0.06	0.02
	Modena	-	-	-	-	-
	Moldova	0.01	0.03	0.04	0.13	0.03
	Moscow MSU	0.01	0.04	0.03	0.05	0.01
	Nes Ziona	0.03	0.07	0.08	0.27	0.06
	Palaiseau	-	-	-	-	-
	Saclay	-	-	-	-	-
	SMHI	0.00	0.01	0.01	0.02	0.01
	Tarbes	0.00	0.01	0.01	0.02	0.01
	Toulouse1	0.01	0.03	0.04	0.12	0.03
	Toulouse2	-	-	-	-	-
	Vinon	0.01	0.01	0.03	0.07	0.01
Remote/Urban Coast	Biarritz	-	-	-	-	-
	Bordeaux	0.01	0.02	0.04	0.11	0.03
	Hamburg	-	-	-	-	-
	IMC Oristano	0.02	0.05	0.07	0.25	0.06
	Marseille	0.01	0.03	0.04	0.09	0.03
	Oostende	0.01	0.04	0.06	0.16	0.05
	Rame Head	-	-	-	-	-
	Realtor	0.01	0.02	0.04	0.26	0.07
	Rome Tor Vergata	0.02	0.04	0.04	0.13	0.03
	Sopot	-	-	-	-	-
	Venise	0.01	0.03	0.04	0.10	0.03
Ocean	Azores	0.01	0.03	0.03	0.06	0.02
	Crete	-	-	-	-	-
	Dead Sea	-	-	-	-	-
	El Arenosillo	0.01	0.04	0.06	0.16	0.04
	Gotland	0.01	0.01	0.02	0.06	0.01
	Helgoland	0.01	0.06	0.05	0.11	0.04
	Kolimbari	-	-	-	-	-
	Lampedusa	0.02	0.06	0.09	0.25	0.07
	Tenerife	-	-	-	-	-
Desert	IMS Metu Erdemli	0.01	0.04	0.06	0.21	0.06
	Sede Boker	0.02	0.06	0.07	0.19	0.04
	Solar Village	0.07	0.16	0.17	0.39	0.08
High Altitude	Clermont Ferrand	-	-	-	-	-
	Davos	0.00	0.01	0.03	0.11	0.04
	Gerlitzen	0.00	0.01	0.02	0.08	0.03
	Izana	-	-	-	-	-
	Pic du Midi	-	-	-	-	-
	Teide	-	-	-	-	-
	Thala	0.01	0.09	0.12	0.36	0.11

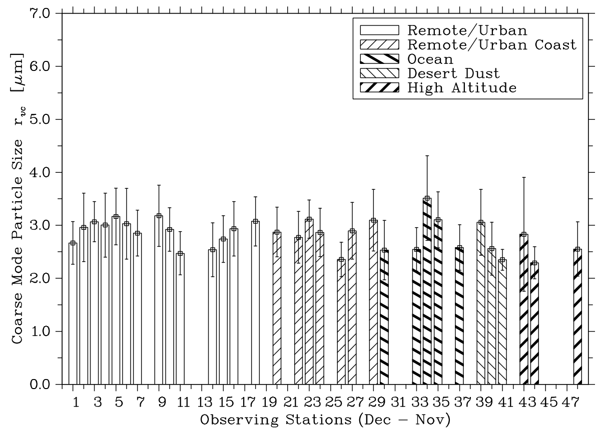

Figure 16: The coarse mode radius for every station. Error bars denote the standard deviation.

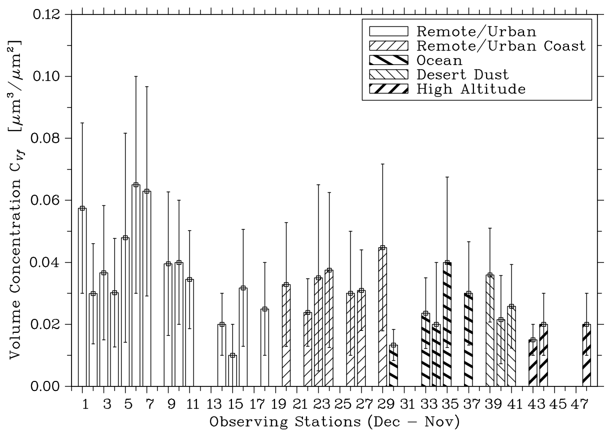

Figure 17: The volume concentration of the fine mode for every station. There are high values in the urban class, which corresponds to the fact that the Ångström coefficient α is higher in that classes.

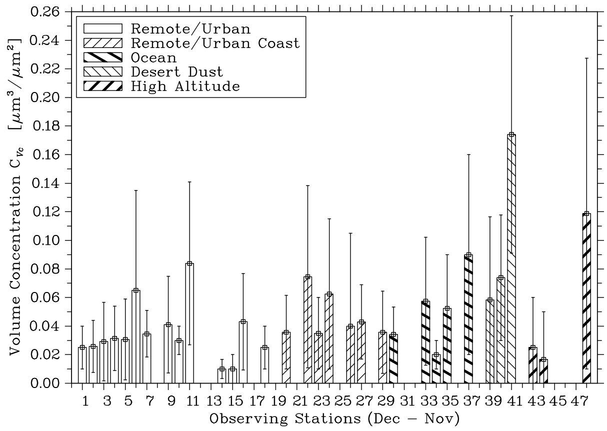

Figure 18: The volume concentration of the coarse mode for every station. There are high values in the desert and ocean class, which corresponds to the fact that the Ångström coefficient α is smaller in that classes.

Table 16: Yearly means of the average monthly means of the median mode radius for the volume particle size distribution for the fine mode and for every class.

Class	N	Min	Med	Mean	Max	Std
R/U	14	0.14	0.16	0.16	0.19	0.02
R/UC	7	0.13	0.16	0.16	0.19	0.02
O	5	0.13	0.16	0.16	0.20	0.02
D	3	0.13	0.15	0.15	0.18	0.02
H. Alt.	3	0.12	0.14	0.15	0.18	0.02

spectively.

9 Single Scattering Albedo and Complex Refractive Index

The single scattering albedo is directly correlated to the imaginary part of the complex refractive index, because if absorption in the aerosol takes place the single scattering albedo is lower than 1. It has been pointed out in chapter 3.2 that the single scattering albedo ω in combination with the reflectance of the ground decides whether cooling or warming will take place in an aerosol layer. Penner *et al.*, 2001 gives for a typical value of ω for a polluted area a value of 0.92 ± 0.05 at 550 nm; values for remote areas goes up to 0.99. Dubovik *et al.*, 2000 reports from single scattering albedos based on the AERONET network, which lie all above 0.9 except

Table 17: Yearly means of the average monthly means of the median mode radius for the volume particle size distribution for the coarse mode and for every class.

Class	N	Min	Med	Mean	Max	Std
R/U	14	2.18	2.89	2.90	3.72	0.50
R/UC	7	2.09	2.86	2.85	3.60	0.46
O	5	2.07	2.81	2.86	3.86	0.55
D	3	2.04	2.64	2.66	3.52	0.44
H. Alt.	3	1.95	2.46	2.56	3.94	0.63

Table 18: Yearly means of the average monthly means of the standard deviation of the median radius of the volume particle size distribution of the fine mode and for every station.

Class	N	Min	Med	Mean	Max	Std
R/U	14	0.62	0.71	0.71	0.81	0.06
R/UC	7	0.60	0.70	0.70	0.81	0.06
O	5	0.55	0.65	0.66	0.79	0.08
D	3	0.56	0.64	0.65	0.73	0.05
H. Alt.	3	0.60	0.72	0.73	0.88	0.09

Table 19: Yearly means of the average monthly means of the standard deviation of the median radius of the volume particle size distribution of the coarse mode and for every station.

Class	N	Min	Med	Mean	Max	Std
R/U	14	0.31	0.35	0.36	0.41	0.03
R/UC	7	0.32	0.37	0.37	0.45	0.04
O	5	0.31	0.38	0.38	0.45	0.04
D	3	0.30	0.36	0.36	0.43	0.04
H. Alt.	3	0.33	0.39	0.39	0.45	0.04

Table 20: Yearly means of the average monthly means of the standard deviation of the volume concentration of the volume particle size distribution of the fine mode and for every station.

Class	N	Min	Med	Mean	Max	Std
R/U	14	0.01	0.03	0.03	0.10	0.03
R/UC	7	0.01	0.03	0.05	0.16	0.04
O	5	0.01	0.04	0.05	0.13	0.04
D	3	0.04	0.09	0.10	0.26	0.06
H. Alt.	3	0.00	0.04	0.05	0.18	0.06

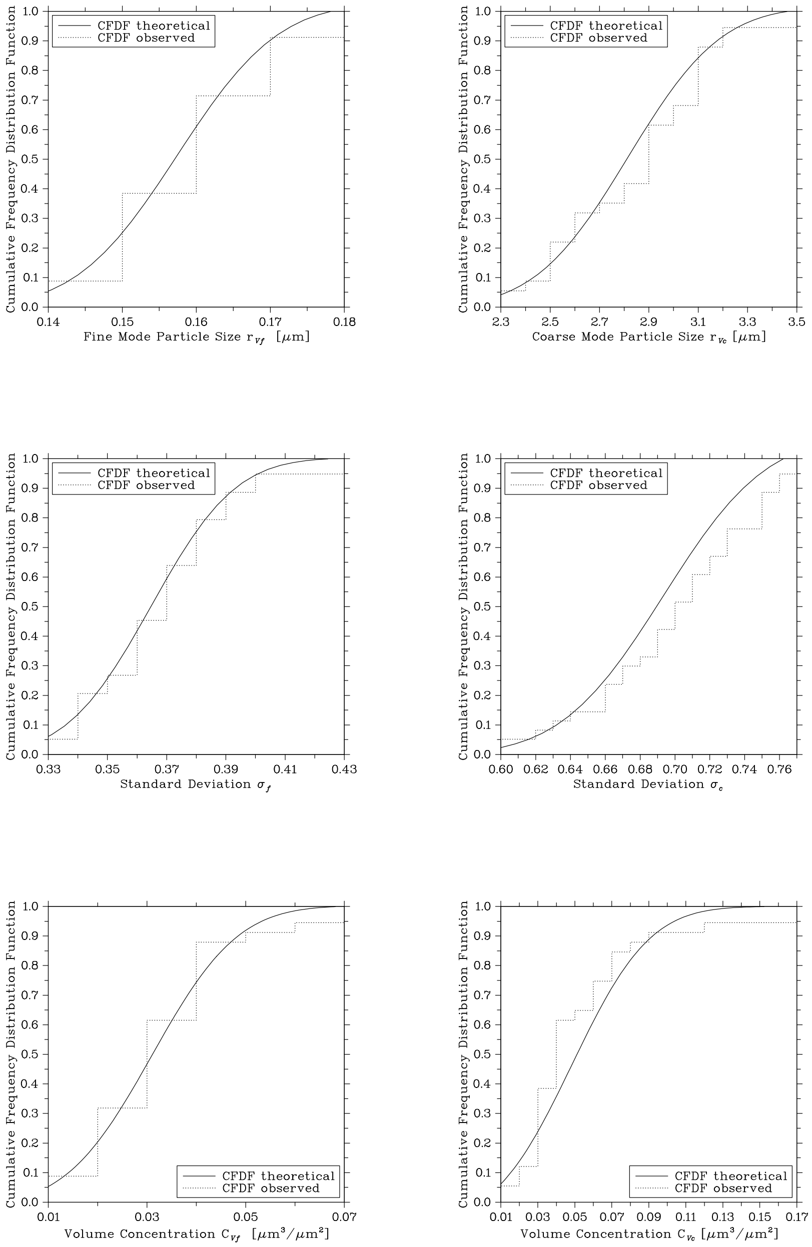

Figure 19: The cumulative frequency distribution function for the radii (fine and coarse mode); the corresponding standard deviations (fine and coarse mode) and the volumes in the fine and coarse mode. Parameters for the theoretical distributions (mean/σ): r_{Vf}: 0.16/0.01; r_{Vc}: 2.83/0.29; σ_f: 0.37/0.02; σ_c: 0.70/0.05; C_{Vf}: 0.03/0.01; C_{Vc}: 0.05/0.03.

Table 21: Yearly means of the average monthly means of the standard deviation of the volume concentration of the volume particle size distribution of the coarse mode and for every station.

Class	N	Min	Med	Mean	Max	Std
R/U	14	0.01	0.03	0.04	0.08	0.02
R/UC	7	0.01	0.03	0.03	0.08	0.02
O	5	0.01	0.02	0.03	0.06	0.02
D	3	0.01	0.03	0.03	0.06	0.01
H. Alt.	3	0.01	0.01	0.02	0.04	0.01

for very polluted areas like Mexico City which has an average single scattering albedo of 0.68 at 440 nm.

Figure 20 shows the single scattering albedo for every station and wavelength. Dubovik *et al.*, 2000 got similar results; especially there is a weak decrease of ω with wavelength in polluted areas; and there is a weak increase of ω with wavelength in arid and desert like locations.

The single scattering albedo is retrieved only then when the aerosol optical depth loading is greater than 0.4 at an wavelength of 440 nm (cf. Dubovik *et al.*, 2000). This means our Gerlitzen station (number 44) will never exhibit any single scattering albedo and complex refractive index values, because the Gerlitzen station is a remote station at an altitude of 2000 m and the aerosol optical values are often quite low there.

Though, Dubovik *et al.*,, 2000 found single scattering values for the Solar Village observing station which are off from ours. Their average single scattering value of the Solar Village station is about 0.92 at 440 nm. We found a single scattering albedo for the Solar Village station of about 0.96 at 440 nm. This difference is possibly due to the different statistical evaluation methods, but the average trend in the urban and desert class remains unaffected by this.

Examples of the statistical parameters for the single scattering albedo at 440 nm are given in Table 22 for each station.

The aerosol optical depth in combination with the single scattering albedo is of great interest for the UV modeler (cf. SUVDAMA 1999). Table 23 exhibits the mean single scattering albedos for every class and every wavelength. It is obvious that ω at 440 nm lies above 0.9, but it does not reach 1.0 due to absorption in the aerosol which takes place over Europe.

One should note that some stations exhibit a rather low single scattering albedo at some days; for example: on the date of June 28, August 3 and 10 of year 2001 Bucharest exhibited a low ω, which is also predominant in the volume particle size distribution. Figure 22 shows the volume particle size distribution for the aforementioned dates of Bucharest. It is obvious that there is a third mode at low particle radius, but one should bear in mind that at these bins the error of the retrieval scheme can reach 100% and more (cf. Dubovik *et al.*, 2000). That is the reason why this third mode has been left out and the mode radius is calculated for the fine

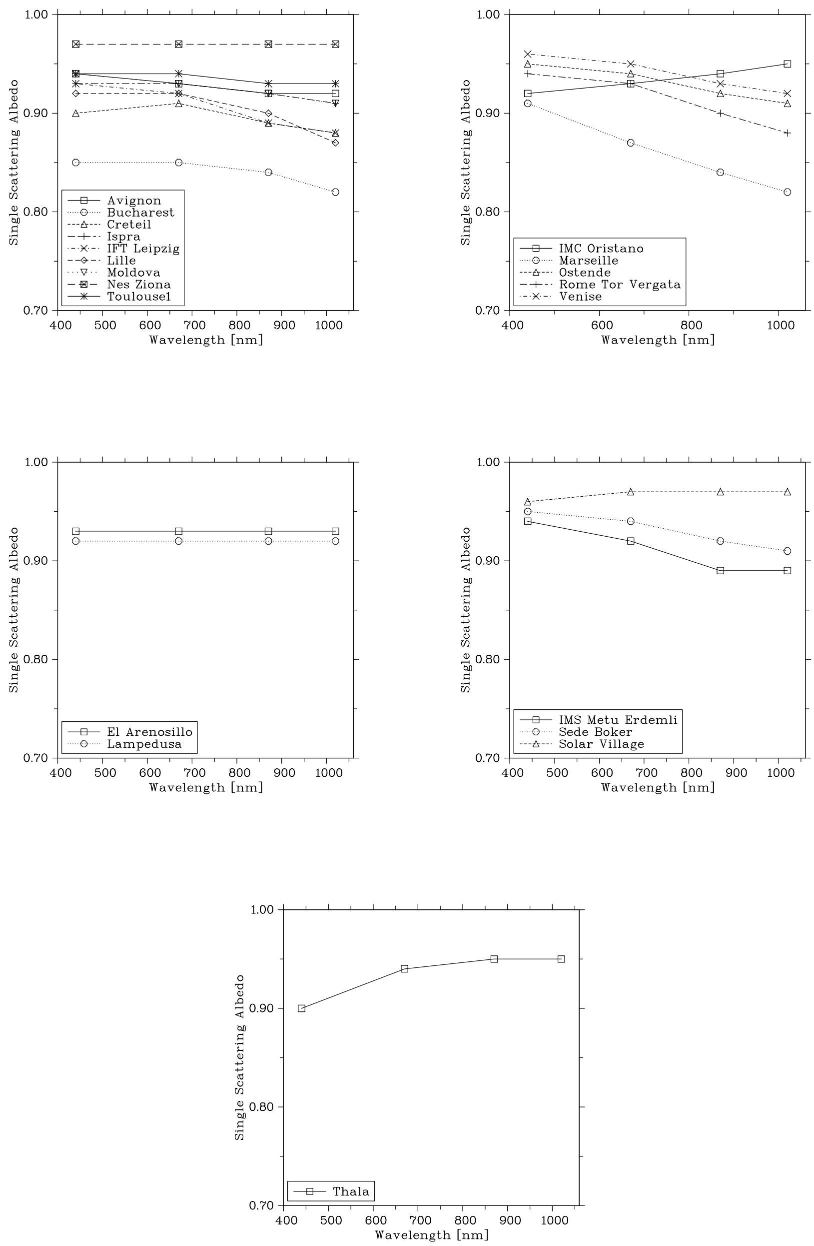

Figure 20: The single scattering albedo for the four wavelengths 440, 670, 870 and 1020 nm. The values are based on the yearly means of the single scattering albedos.

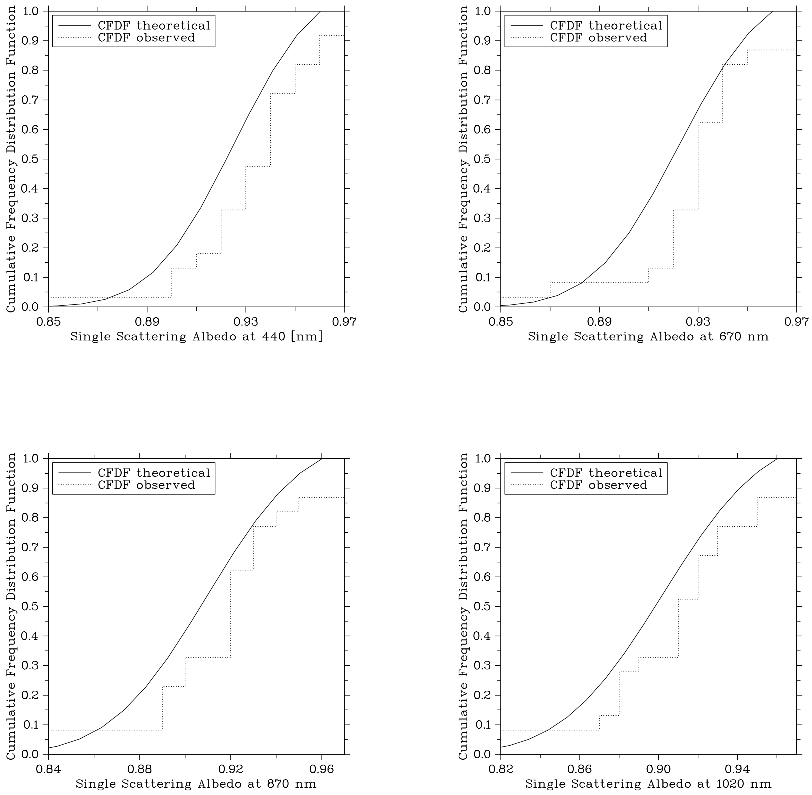

Figure 21: The cumulative frequency distribution function for the single scattering albedo and four wavelengths, respectively. Parameters for the theoretical distributions (mean/σ): ω_{440}: 0.93/0.03; ω_{670}: 0.93/0.03; ω_{870}: 0.91/0.03; ω_{1020}: 0.91/0.04. The parameters are based on the yearly mean values of Table 22.

Table 22: Yearly means for the average statistical parameters of the single scattering albedo at 440 nm.

	Station	Min	Med	Mean	Max	Std
Remote/Urban	Aire Adour	-	-	-	-	-
	Avihharest	0.91	0.95	0.94	0.95	0.02
	Bucarest	0.61	0.90	0.85	0.93	0.13
	Creteil	0.87	0.91	0.90	0.93	0.02
	Ispra	0.91	0.94	0.93	0.96	0.02
	IFT Leipzig	0.92	0.93	0.93	0.95	0.01
	Lille	0.83	0.94	0.92	0.96	0.06
	Modena	-	-	-	-	-
	Moldova	0.91	0.93	0.94	0.96	0.02
	Moscow MSU	-	-	-	-	-
	Nes Ziona	0.93	0.97	0.97	0.98	0.02
	Palaiseau	-	-	-	-	-
	Saclay	-	-	-	-	-
	SMHI	-	-	-	-	-
	Tarbes	-	-	-	-	-
	Toulouse1	0.91	0.95	0.94	0.96	0.02
	Toulouse2	-	-	-	-	-
	Vinon	-	-	-	-	-
Remote/Urban Coast	Biarritz	-	-	-	-	-
	Bordeaux	-	-	-	-	-
	Hamburg	-	-	-	-	-
	IMC Oristano	0.90	0.90	0.92	0.99	0.04
	Marseille	0.86	0.91	0.91	0.94	0.03
	Oostende	0.93	0.95	0.95	0.98	0.02
	Rame Head	-	-	-	-	-
	Realtor	-	-	-	-	-
	Rome Tor Vergata	0.92	0.94	0.94	0.96	0.01
	Sopot	-	-	-	-	-
	Venise	0.94	0.96	0.96	0.98	0.01
Ocean	Azores	-	-	-	-	-
	Crete	-	-	-	-	-
	Dead Sea	-	-	-	-	-
	El Arenosillo	0.91	0.93	0.93	0.95	0.01
	Gotland	-	-	-	-	-
	Helgoland	-	-	-	-	-
	Kolimbari	-	-	-	-	-
	Lampedusa	0.89	0.91	0.92	0.95	0.02
	Tenerife	-	-	-	-	-
Desert	IMS Metu Erdemli	0.91	0.94	0.94	0.96	0.02
	Sede Boker	0.93	0.95	0.95	0.97	0.01
	Solar Village	0.93	0.96	0.96	0.98	0.02
High Altitude	Clermont Ferrand	-	-	-	-	-
	Davos	-	-	-	-	-
	Gerlitzen	-	-	-	-	-
	Izana	-	-	-	-	-
	Pic du Midi	-	-	-	-	-
	Teide	-	-	-	-	-
	Thala	0.85	0.90	0.90	0.95	0.03

Table 23: Yearly means of the average yearly means of the single scattering albedo for every class at the wavelengths of 440, 670, 870 and 1020 nm.

440 nm						
Class	N	Min	Med	Mean	Max	Std
R/U	9	0.87	0.94	0.92	0.95	0.03
R/UC	5	0.91	0.93	0.94	0.97	0.02
O	2	0.90	0.92	0.93	0.95	0.02
D	3	0.92	0.95	0.95	0.97	0.02
H. Alt.	1	0.85	0.90	0.90	0.95	0.03
670 nm						
Class	N	Min	Med	Mean	Max	Std
R/U	9	0.87	0.93	0.92	0.96	0.03
R/UC	5	0.89	0.92	0.92	0.96	0.03
O	2	0.90	0.93	0.93	0.95	0.02
D	3	0.91	0.94	0.94	0.96	0.02
H. Alt.	1	0.92	0.95	0.94	0.97	0.02
870 nm						
Class	N	Min	Med	Mean	Max	Std
R/U	9	0.84	0.92	0.91	0.95	0.04
R/UC	5	0.85	0.90	0.91	0.96	0.03
O	2	0.88	0.92	0.93	0.95	0.03
D	3	0.89	0.93	0.93	0.96	0.02
H. Alt.	1	0.93	0.95	0.95	0.97	0.02
1020 nm						
Class	N	Min	Med	Mean	Max	Std
R/U	9	0.83	0.90	0.90	0.95	0.05
R/UC	5	0.84	0.89	0.90	0.95	0.04
O	2	0.88	0.92	0.93	0.96	0.03
D	3	0.88	0.92	0.92	0.96	0.03
H. Alt.	1	0.93	0.95	0.95	0.98	0.02

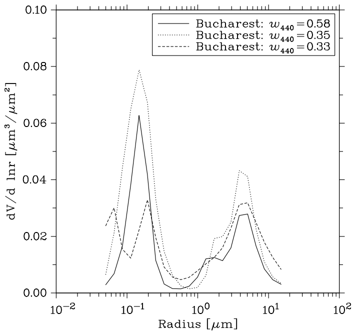

Figure 22: The volume particle size distribution for the three days, where Bucarest exhibited a very low single scattering albedo. In this case a third mode appears in one of the observations, which is very questionable (refer to text for more details).

and coarse mode alone. Figure 21 exhibits the cumulative frequency distribution function for the single scattering albedo and their respective wavelengths.

9.1 Complex Refractive Index

The particle distribution in combination with the complex refractive index leads to the single scattering albedo and phase function of the scattering and absorbing aerosol. Figures 23 and 24 exhibit the real and imaginary part of the observing station in every class for different wavelengths. Dubovik *et al.*, 2001 pointed out, that a wavelength-dependent increase of the real part of the refractive index corresponds to non-spherical particles. It can be highly misleading to use in a first step the value of the real part at 440 nm and guess that it will be constant along the wavelength (cf. Köpke *et al.*, 1997).

Due to the highly unclear accuracy of the real and imaginary part of the refractive index no average values for the typical class are given.

10 Discussion

The findings presented in the last chapters can serve as input for studies in the UV-regime. In the UV the problem actually is, that there are very few observations made in order to retrieve the aerosol optical depth and other parameters. The common way thus far is to try to deduce the influence of aerosols in the UV section with the measurements made in the visible part of the solar spectrum. The AERONET network operates mainly in the visible part of the solar spectrum. Though there are the possibility to observe at 340 nm with the CIMEL CE-318, but the measurements are scarce there.

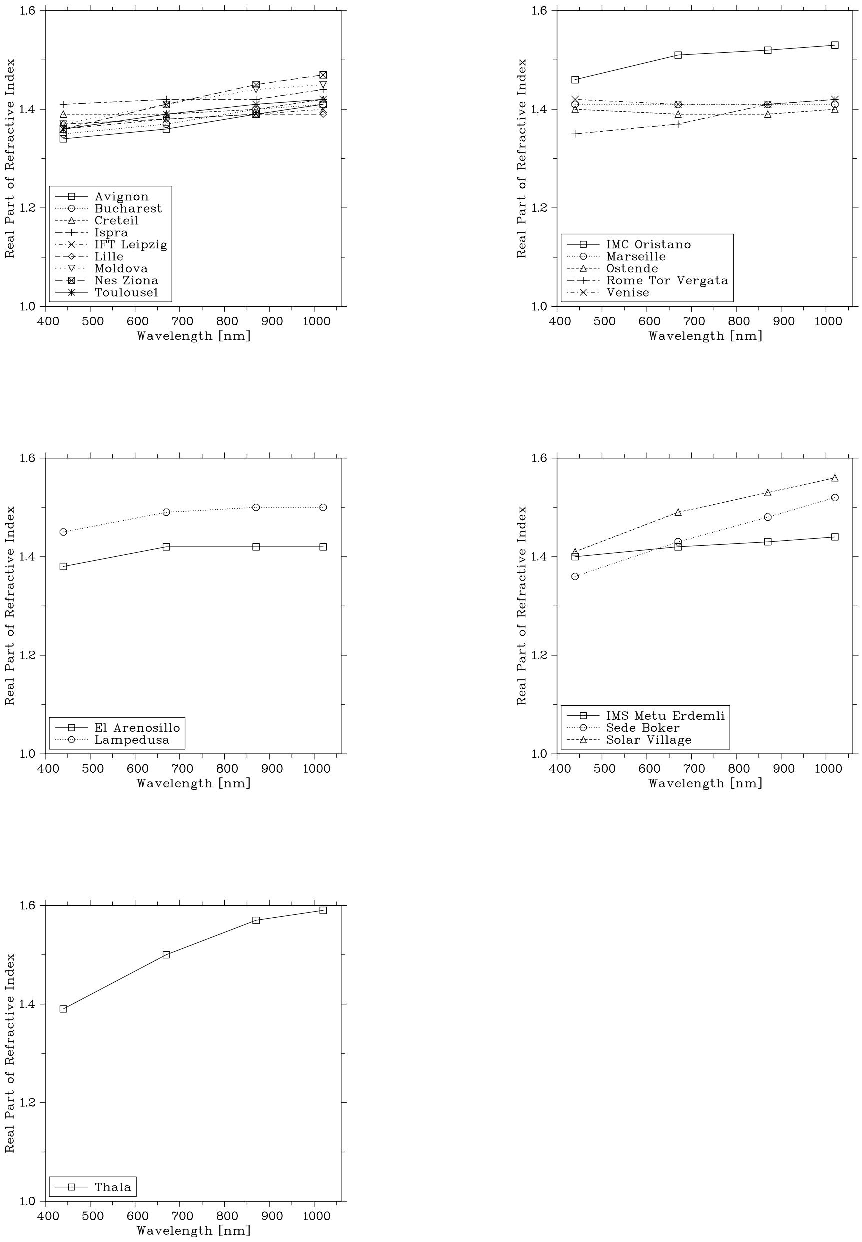

Figure 23: The real part of the complex refractive index for the four wavelengths 440, 670, 870 and 1020 nm. The values are based on the yearly means of the real part of the complex refractive index.

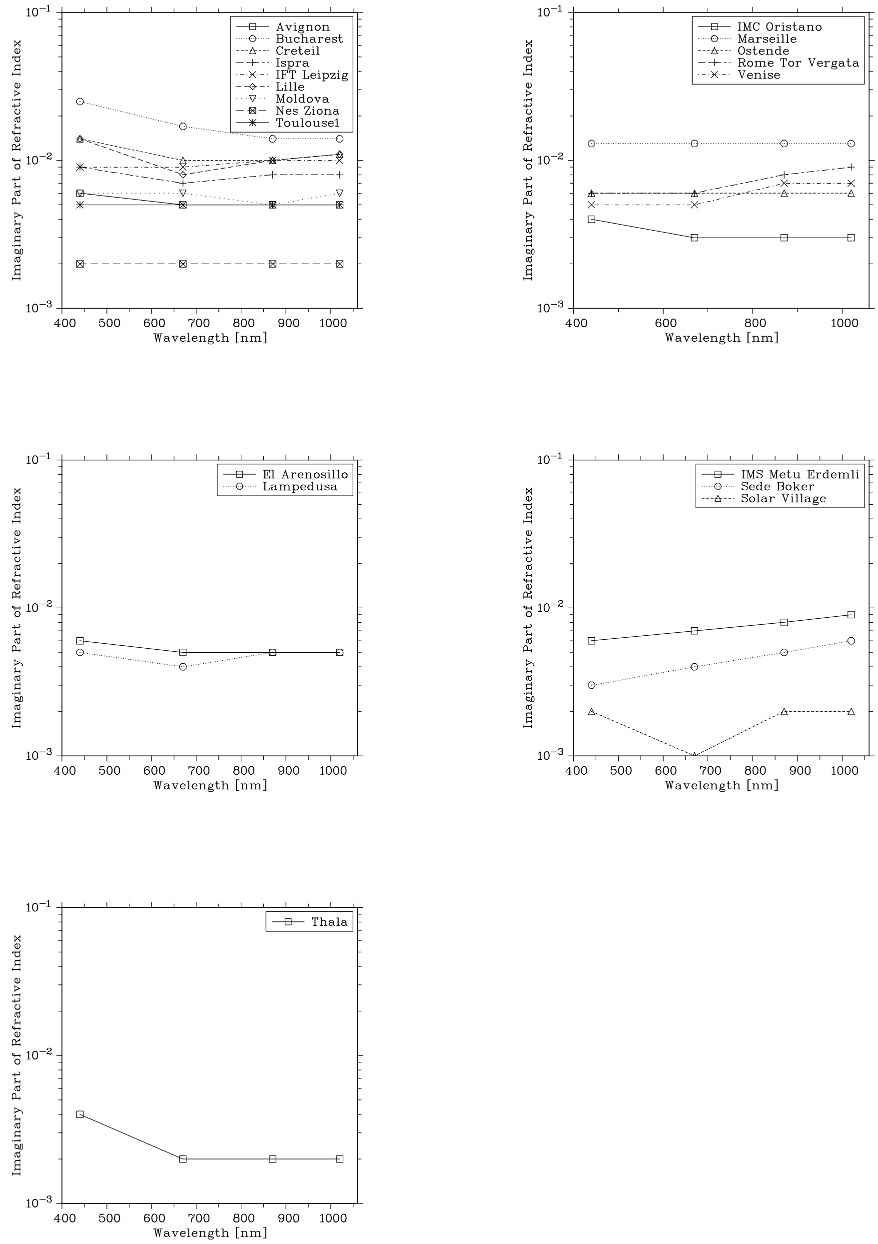

Figure 24: The imaginary part of the complex refractive index for the four wavelengths 440, 670, 870 and 1020 nm. The values are based on the yearly means of the imaginary part of the complex refractive index.

Table 24: The aerosol optical depth at the wavelength of 312 nm due to the aerosol optical depth at 440 nm and the Ångström coefficient α deduced from the observations in 440 and 870 nm. τ_{440} and α is based on the AERONET observations over Europe.

Class	τ_{440}	α	τ_{312}	UV-B transmission [%]
R/U	0.27	1.36	0.43	82
R/UC	0.24	1.33	0.38	83
O	0.23	1.01	0.33	83
D	0.28	1.03	0.4	82
H. Alt.	0.11	1.24	0.17	85

Wenny *et al.*, 1998 found a linear relationship between the aerosol optical depth at 415 and 500 nm. According to their work an aerosol optical depth of about 0.55 at 415 nm should result in a decrease of the UV-B transmission of 30%. That is somewhat in contrast to the work of Mayer 1997, who estimates a maximal decrease of the UV-B (280 - 315 nm) transmission of 18% at an aerosol optical depth of 0.7 at 340 nm. Köpke 2002 obtained similar results insofar that he assumes that the UV-B radiation can be reduced at maximum by 35% due to aerosol particles (cf. Köpke 2002).

The SUVDAMA end report (cf. SUVDAMA 1999) supports also the thesis that aerosols and single scattering albedo can have a great influence on the attenuation of UV radiation. The findings of their respective SUVDAMA contributors vary strongly, but nobody assumes that the UV-B radiation is attenuated due to aerosols by more than 35%.

The above finding would point to an interesting fact that possibly the aerosol influence on UV radiation is greater than expected.

Theoretically one can calculate the optical depth with the help of the Ångström coefficient; but it is unlikely that the Ångström coefficient α is really the appropiate tool to extrapolate into the UV regime. For example, if one knows the aerosol optical depth at 440 nm one could calculate the aerosol optical depth at different wavelength in the UV. Table 24 presents the aerosol optical depth at the wavelengths of 312 nm for the average yearly aerosol optical depth and their respective Ångström coefficient α for the different location classes.

Wenny *et al.*, 1998 gives an estimate of the UV-B transmission at solar noon and their decrease due to influence of aerosols at solar noon:

$$ln(UV - B \quad transmission) = -0.1422(\tau_{312}) - 0.138 \tag{13}$$

The values in Table 24 for the transmission in the UV-B range should not be taken too literally, because Wenny *et al.*, 1998 made the measurements at one specific location and our aerosol optical depth at 312 nm is based on the Ångström coefficient, which could overestimate the aerosol optical depth. But one can be sure that the aerosol optical depth lies between the value of τ at 440 nm and τ at the calculated wavelength (312 nm in the above case). There is no clear method

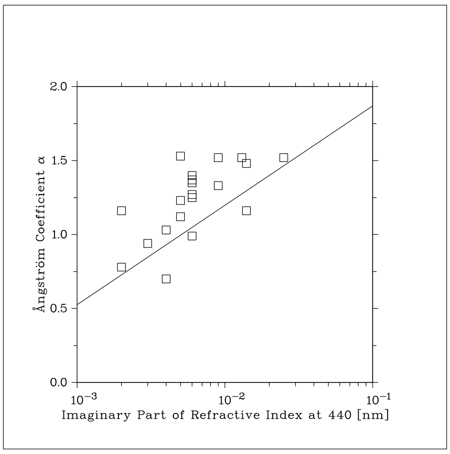

Figure 25: The Ångström coefficient versus the imaginary part of the complex refractive index. There is a weak linear relationship between the two parameters. The parameters of the relation are: correlation coefficient: 0.66; $y = log_{10}(x)tan(0.59) + 2.54$.

(cf. Köpke 2002) or theory which could explain the behaviour of the aerosol optical depth extrapolated into the UV regime.

Interesting to note here is the finding that the transmission attenuation is nearly as constant over Europe. But one may not forget that the above estimation is based upon the mean, average aerosol optical depth for every class, which in turn is the sum of all members; it is therefore likely that there exists quite great deviations between observing stations.

The single scattering albedo is the second most important parameter in order to describe UV-radiation in radiative transfer codes (cf. SUVDAMA 1999). The AERONET network delivers the single scattering albedo for specific locations. But one could also get the single scattering albedo ω if one applies the Mie theory to the complex refractive index and particle radius. It is not unlikely that the single scattering albedo as retrieved from the AERONET network will differ from the single scattering albedo retrieved from the Mie code due to assumptions on the particle distribution; the AERONET network retrieves the single scattering albedo due to an inversion algorithm (cf. Dubovik *et al.*, 2000).

Actually the great hindrance is to decide whether the single scattering albedo will remain constant in the UV part of the spectrum or not. As one can see from Figure 20, ω exhibits a weak linear relationship with the wavelength (except for the desert and arid case); it is not clear whether the trend will go linear through the UV regime. In a first guess one could use the single scattering albedo value at 440 nm and guess that it will stay valid in the UV part.

We have tried to find relationships between the Ångström coefficient α, aerosol optical depth, single scattering albedo, complex refractive index and particle radius. There is only one case where one could guess a linear relationship, and that was between the Ångström coefficient and the imaginary part of the refractive index.

Figure 25 shows α versus the imaginary part of the refractive index. The correlation coefficient of 0.7 is not very high but one can see a weak linear trend between the two parameters. Figure 25 indirectly supports the proposition mentioned elsewhere in the report that a high Ångström coefficient is correlated with small smoke particles and in turn small smoke particles are often predominant in polluted areas where the imginary part of the refractive index (absorption coefficient) is quite high.

11 Conclusion

A statistical evaluation of the AERONET network operating in Europe has been presented. The most important aerosol paramaters for the UV modeler are the aerosol optical depth, Ångström coefficient and single scattering albedo. It is not clear yet whether it is possible to use the Ångström coefficient in order to extrapolate the aerosol optical depth into the UV region. But the Ångström coefficient is an essential tool in order to make an assessment of the aerosol optical depth in the UV region. It turned out that the mode radius of the particle volume size distribution is nearly constant among the different stations. That can be attributed to the inversion algorithm or the fact that Europe is a small area and that the principal contributors to the aerosol population show a similar particle dimension from station to station. It was demonstrated that the aerosol optical depth load in the summer months are higher than in the winter months. That is what can be expected from observations in the past; but there is also the caveat that under certain circumstances the retrieval algorithm does not work best, because it applies a table lookup value for the ground albedo, which does not describe the actuall environment of the observing station.

The single scattering albedo displays a similar behavior for all non-desert like areas. The desert-like class is affected by non-spherical particles which the retrieval algorithm cannot deduce. The findings for the desert class should be seen with some remarks of caution. It interesting to note that the single scattering albedo lies above 0.91 for most of the observing stations; Bucharest is the exception which can be attributed to a very polluted area or some form of soot occurence. The values for the single scattering albedo agrees well with findings of other researchers. The findings of the AERONET stations are nessecarily important, because it is always best to confirm the results from theoretical considerations with results from observations.

The interested reader can obtain more data for other wavelength channels than 440 nm from the corresponding author adress: siegfried.gonzi@kfunigraz.ac.at

Acknowledgments. We thank the PI investigators and their staff for establishing and maintaining of the 48 European AERONET sites used in this report.

References

[1] Boucher, O., 1997: *On the Aerosol Direct Shortwave Forcing and the Henyey-Greenstein Phase Function,* J.Atmos.Sci., 55, 128 - 134.

[2] Coakly, J.A., et al., 1983: *The Effect of Tropospheric Aerosols on the Earth's Radiation Budget: A Parameterization for Climate Models,* J.Atmos.Sci, 40, 116 - 138.

[3] Dubovik, O., et al., 2000: *Accuracy assessments of aerosol optical properties retrieved from Aerosol Robotic Network (AERONET) Sun and sky radiance measurments,* JGR, 105, 9791 - 9806.

[4] Dubovik, O.,et al., 2002: *Variability of Absorption and Optical Properties of Key Aerosol Types Observed in Worldwide Locations,* J. Atmos. Sci., 59, 590 - 608.

[5] Eck, T.F., et al., 1999: *Wavelength dependence of the optical depth of biomass burning, urban, and desert dust aerosol,* JGR, 104, 31,333 - 31,350.

[6] Gonzales, C.R., et al., 2000: *Aerosol optical depth over Europe in August 1997 derived from ATSR-2 data,* GRL, 27, 955 - 958.

[7] Guzzi, R., et al., 2001: *Aerosol maps from GOME data,* Atm. Env., 35, 5079 - 5091.

[8] Haywood, J.M., Shine, K.P., 1995: *The effect of anthropogenic sulfate and soot aerosol on the clear sky planetary radiation budget,* GRL, 22, 603 - 606.

[9] Haywood, J. M., Ramaswamy, V., 1998: *Global sensitivity studies of the direct radiative forcing due to anthropogenic sulfate and black carbon aerosols,* JGR, 103, 6043 - 6058.

[10] Haywood, J., Boucher, O., 2000: *Estimates of the direct and indirect radiative forcing due to tropospheric aerosols: A review,* Rev. Geoph., 38, 513 - 543.

[11] Herman, M., et al., 1997a: *Remote sensing of aerosols over land surfaces including polarization measurements and application to POLDER measurements,* JGR, 102, 17,039 - 17,049.

[12] Herman, M., et al., 1997b: *Remote sensing of aerosols over land surface including polarization measurments and application to POLDER measurements,* JGR, 102, 17,039 - 17,049.

[13] Herman, J.R., et al., 1997c: *Global distribution of UV-absorbing aerosols from Nimbus 7/TOMS data,* JGR, 102, 16,911 - 16,922.

[14] Hess, M., et al., 1998: *Optical Properties of Aerosols and Clouds: The Software Package OPAC,* B. Am. Met. Soc., 79, 831 - 844.

[15] Hsu, N.C., et al., 1999: *Comparison of the TOMS aerosol index with Sun-photometer aerosol optical thickness: Results and applications,* JGR, 104, 6269 - 6279.

[16] Holben, B.N., et al., 1998: *AERONET - A Federated Instrument Network and Data Archive for Aerosol Characterization,* Remote Sens. Environ., 66, 1 - 16.

[17] Holben, B.N., et al., 2001: *An emerging ground-based aerosol climatology: Aerosol optical depth from AERONET,* JGR, 106, 12,067 - 12,097.

[18] Husar, R.B., et al., 2000: *Distribution of continental surface aerosol extinction based on visual range data,* Atmos. Env., 34, 5067 - 5078.

[19] Isaaks, E.H., Srivastava, R.M., 1989: *An Introduction to Applied Geostatistics,* Oxford University Press, ISBN 0-19-505013-4.

[20] Kaufman, Y.J., Holben, B.N., 1996: *Hemispherical backscattering by biomass burning and sulfate particles derived from sky measurements,* JGR, 101, 19,433 - 19,445.

[21] Kerry, K.E., Hawick, K.A., 1998: *Kriging Interpolation on High-Perfromance Computers,* Proc. of High Perfromance Computing and Network (HPCN) Europe '98, Amsterdam 1998.

[22] King, M.D., et al., 1999: *Remote Sensing of Tropospehreic Aerosols from Space: Past, Present, and Future,* B. Am. Met. Soc., 2229 - 2259.

[23] Köpke, P., et al., 1992: *Climate Effetcs of Atmospheric Aerosols,* Nucleation and Atmospheric Aerosols, N. Fukuta and E. Wagner (eds.), ISBN 0-937194-26-3.

[24] Köpke, P., et al., 1997: *Global Aerosol Data Set,,* Max-Planck-Institut für Meteorologie Report No. 243, ISSN 0937-1060.

[25] Köpke, P., 2002: *Private Communication,* corresponding author adress: P. Köpke, Meteorologisches Institut der Universität München, Theresienstr. 37, D-80333 München, Germany.

[26] Krekov, G.M., 1992: *Models of atmospheric aerosols,* in Aerosol Effects on Climate, Jennings (editor), The University of Arizona Press, ISBN 0-8165-1362-7.

[27] Lakis, A., et al., 1992: *Climate Forcing by Stratospheric Aerosols,* GRL, 19, 1607 - 1610.

[28] Mayer, B., 1997: *Messung und Modellierung der spektralen UV-Bestrahlungsstärke in Garmisch-Partenkirchen,* Dissertation, Schriftenreihe des Fraunhofer-Instituts für Atmosphärische Umweltforschung, Band 45, ISBN 3-927548-94-4.

[29] Michalsky, J.J., et al., 2001: *Multiyear measurements of aerosol depth in the Atmospheric Radiation Measurments and Quantitative Links programs,* JGR, 106, 12,099 - 12,107.

[30] Nemesure, S., et al., 1995: *Direct shortwave forcing of climate by the anthropogenic sulfate aerosol: Sensitivity to particle size, composition, and relative humidiyt,* JGR, 100, 26,105 - 26,116.

[31] Penner, J.E., et al., 2001: *Aerosols, their Direct and Indirect Effects,* IPCC, Climate Change 2001, The Scientific Basis, Chapter 5, 289 - 348.

[32] Plinis, C., et al., 1995: *Sensitivity of Direct Climate Forcing by Atmospheric Aerosols to Aerosol Size and Composition,* JGR, 100, 18,739 - 18,754.

[33] Remer, L.A., et al., 1998: *Biomass burning aerosol size distribution and modeled optical properties,* JGR, 103, 31,879 - 31,891.

[34] Seinfeld, J.H., Pandis, S.N., 1998: *Atmospheric Chemistry and Physics,* John Wiley & Sons, Inc., ISBN 0-471-17816-0.

[35] Smirnov, A., et al., 2000: *Cloud screening and quality control algorithms for the AERONET database,* Rem.Sens.Environ., 73, 337 - 349.

[36] SUVDAMA, 1999: *Scientific UV Data Management (SUVDAMA) for teh period March 1996 - June 1999,* Contract No. ENV4-CT95-0177.

[37] Tanre, D., et al., 2001: *Global observation of anthropogenic aerosols from satellite,* GRL, 28, 4555 - 4558.

[38] Torres, O., et al., 1998: *Derivation of aerosol properties from satellite measurements of backscattered ultraviolet radiation: Theoretical basis,* JGR, 103, 17,099 - 17,110.

[39] Tranchant, B.J.S., Vincent, A.P., 2000: *Statistical interpolation of ozone measurements from satellite data (TOMS, SBUV and SAGE II9 using kriging method,* Ann. Geophysicae, 18, 666 - 6784.

[40] Wenny, B.N., et al., 1998: *A Study of Regional Aerosol Radiative Properties and Effects on Ultraviolett-B Radiation,* JGR, 103, 17,083 - 17,097.

[41] Wiscombe, W.J., Grams, G.W., 1976: *The Backscattered Fraction in Two-Stream Approximations,* JGR,33, 2440 - 2451.

[42] Wilks, D.S., 1995: *Statistical Methods in the Atmospheric Sciences,* Academic Press, ISBN 0-12-751965-3.